

Report for SKY project

Pulp Mill Deposit Formation and Aging – Role of Intra-Deposit Alkali Chloride Transport – Phase 2

Roland Balint, Markus Engblom

Åbo Akademi University

08.12.2021

Executive summary

The objective of the work reported here is to better understand changes in deposit chemistry due to the deposit temperature gradient and as a function of time. These changes take place after the initial deposit formation and will be referred to as deposit ageing in the further course of this report. Identifying and understanding the underlying mechanisms responsible for local changes within the deposit chemistry is of great importance when predicting a deposit's melting behaviour and morphology, thus being able to estimate the corrosiveness and also the removability of deposits.

This report summarizes the work carried out and results obtained from probe measurements in the Rauma recovery boiler. The current probe measurements (phase 2) are a continuation of an earlier SKY project aimed at probe development (phase 1). The phase 2 probe data is in this report complemented by observations and understanding gained from other work. Laboratory experiments, as well as data from deposits collected directly from boiler superheaters in Finland and in Brazil are presented to obtain a more comprehensive overall picture of how recovery boiler deposits change in chemical composition and morphology with time and due to the temperature gradient present over the deposit.

Based on the overall body of knowledge gained from laboratory experiments, boiler deposit sampling, and probe measurements it can be concluded that

- **Cl enrichment in Finnish superheater deposits takes place with time.** Both local enrichment, forming Cl-rich layers within the deposit, but also a general increase in the bulk Cl content of the deposits takes place over time.
- Both boiler deposit samples and probe deposits show **a local decrease in T_0 close to the steel compared to the bulk deposit, which can be expected to increase the risk of corrosion with time.**

The composition differences resulting in these locally lower T_0 values can either be set up during initial deposit build-up stages (condensation of alkali chloride vapours on steel surface) and/or due to time-dependent changes within the deposit after the deposit has built up. In both cases, the mechanism is vaporization-condensation of alkali chlorides.

In Finnish mill deposits, vaporization and condensation and gas-phase alkali chloride transport appear to be the main mechanism by which the deposit can be enriched in alkali chlorides, both locally and as a whole. In contrast, Brazilian deposits have higher Cl compared to typical Finnish/Scandinavian mills. The higher Cl of Brazilian deposits results in additional deposit ageing mechanisms becoming relevant.

In the Brazilian deposits studied, movement of an alkali chloride-rich melt toward the steel resulted in locally lower T_0 values toward the steel. In addition, gas phase alkali chloride transport could clearly be seen to have taken place in the Brazilian deposits as well. The lowest local T_0 value found in the Brazilian deposits (517 °C) was slightly lower as compared to the lowest T_0 value in the Finnish superheater deposit (522 °C). In both the Brazilian and Finnish superheater deposits, the lowest local T_0 values were typically found in the region relatively close to the steel surface.

The Rauma probe measurements also provided observations of new deposit characteristics to be understood better in future work. Similar observations were also made in the deposit samples collected directly from the superheaters in the Rauma boiler.

Introduction

Intensive research on kraft recovery boiler deposits has been carried out over the last decades by various research groups. Thus the composition and build-up mechanisms of superheater deposits are well known and understood by now.[1–5] One result of this early research has been the identification of specific temperatures which are nowadays well accepted and used in industry when designing new boilers and for modelling calculations concerning deposit formation in the superheater region of a recovery boiler.[5–7] The main characteristic temperatures are best to be explained by taking a closer look at the melting behaviour of a deposit. Figure 1 shows the temperature-dependent amount of melt formed in a superheater deposit with a composition typical for Finnish / Nordic kraft recovery boilers.

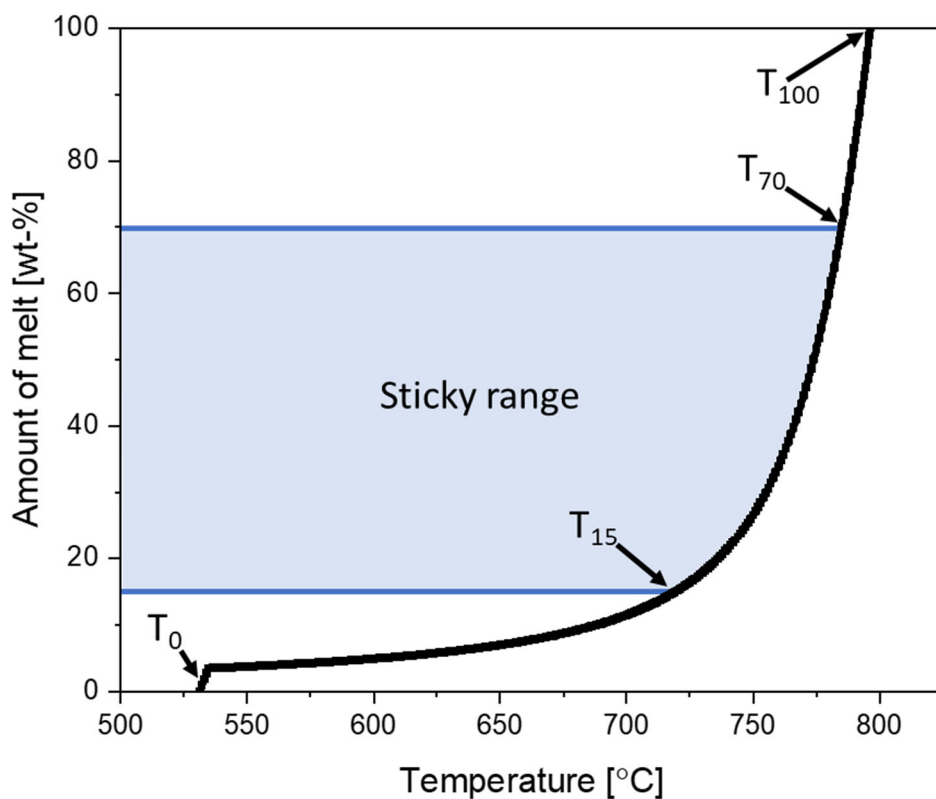


Figure 1: Melting behavior of typical Finnish (Nordic) recovery boiler superheater deposit with characteristic temperatures indicated

As the deposits consist of various compounds, mainly NaCl, Na₂SO₄, Na₂CO₃ and their potassium counterparts, melting takes place over a wider temperature range. Using the graph shown in Figure 1, characteristic melting temperatures can be explained the best. At a certain temperature, which is composition-dependent, the deposit starts melting. The first melting temperature is typically referred to as T_0 and plays an important role for boiler operators as the steel temperature of the heat transfer surfaces should at no time reach values above T_0 of the deposit to avoid severe melt-induced corrosion. With increasing temperature, the melt-fraction within the deposit increases. The next characteristic temperature will be reached as the amount of melt reaches 15 wt-%, thus commonly referred to as T_{15} . At T_{15} , the amount of melt present in the deposit is sufficient to result in a sticky deposit surface enabling further deposition of ash particles, thus enabling fast deposit build-up rates. [7] Deposits are considered to be sticky up to a melt-fraction of 70 wt-%, which is commonly referred to as T_{70} in

literature. Therefore, the temperature region between T_{15} and T_{70} has been established to be called the sticky range and rapid deposit growth can be expected in this temperature range. At temperatures above T_{70} , the main fraction of the deposit will be in molten state, thus slagging of deposits will occur. Furthermore, with amounts of melt as high as 70 wt-% or above, the rather liquid deposit does not adhere well enough to the steel surface anymore but will flow off the superheaters meaning that the deposit has reached a maximum thickness at a temperature of T_{70} at the outer deposit surface. [5,6] The last characteristic temperature to be mentioned here is T_{100} , at which the deposit is fully molten.

A second significant outcome of research that has been carried out in the past is the insights gained on the impact of Cl and K on the melting behaviour of superheater deposits. Figure 2 shows the calculated melting behaviour of model deposits that have higher concentrations in K, Cl, or both compared to the deposit composition of a typical Finnish superheater, indicated in the figure by the black melting curve.

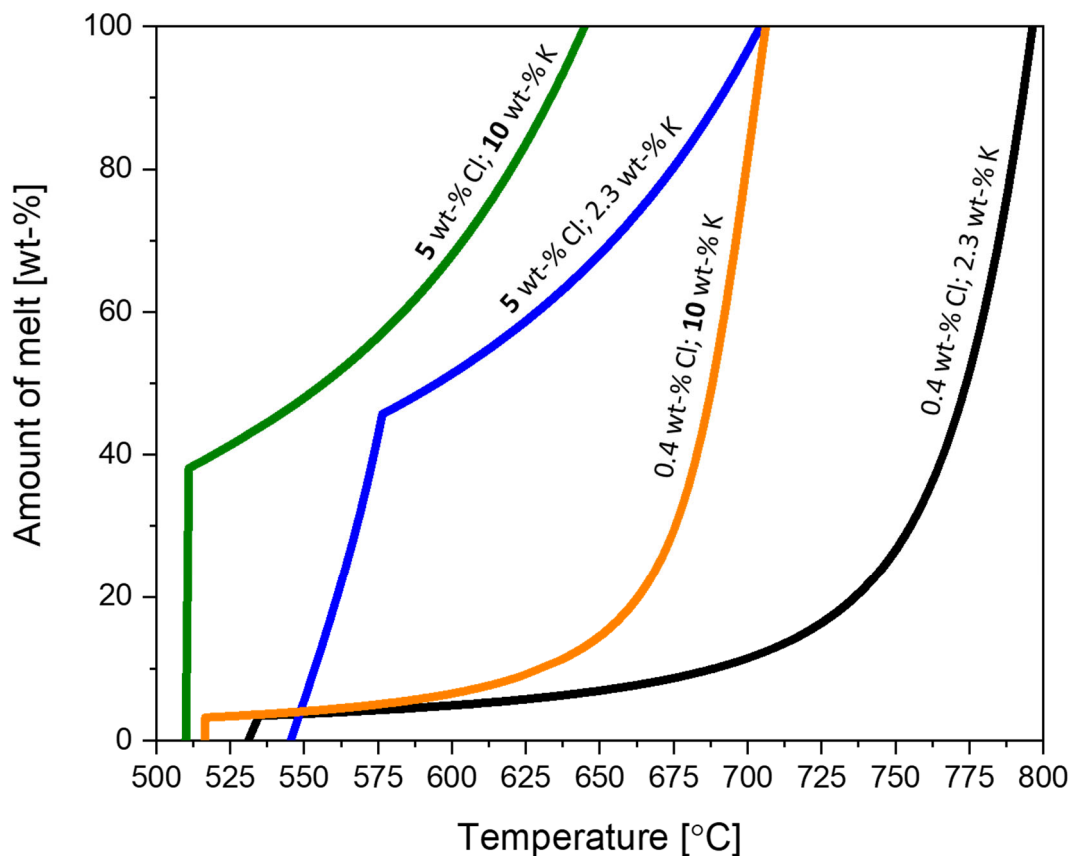


Figure 2: Melting behaviour of deposits enriched in Cl (blue), K (orange), or both (green) compared to a typical Nordic superheater deposit (black)

The three melting curves of the enriched deposits in Figure 2 differ significantly from one another and also from the base case of a typical Finnish superheater deposit. The differences seen are caused by the differences in the K and Cl content of the deposits. Generally, Cl has been identified to affect the amount of melt formed.[8] High concentrations in Cl result in high amounts of melt being formed already at or close to T_0 . When comparing the deposits high in Cl shown in Figure 2 with the typical deposit of a Finnish kraft recovery boiler, the amount of melt formed at T_0 within the Cl enriched deposits is more than ten times higher than in the deposit typical for a Finnish kraft recovery boiler. The K content in deposits on the other hand influences the first melting temperature T_0 . With increasing K content, the first melting temperature decreases.[8] Thus both Cl and K play a vital role in deposit chemistry and will also be a key point of interest in the present report. It can also be seen in Figure 2 that simultaneous enrichment in both K and Cl lowers the first melting temperature even

further when compared to the deposit only enriched in K. It has been shown in literature, that an increase in Cl at concentrations up to 5 mol-% results in an additional decrease in the first melting temperature.[8]

Besides the melting behaviour, also deposition mechanisms of kraft recovery boiler superheater deposits have been studied thoroughly over the last decades, which has led to a good general understanding of the deposit formation mechanisms and which particle size fractions contribute to what extent in the deposit build-up. [1,4,5,9] In the flue gas of a kraft recovery boiler, various particle sizes are present. This in turn results in different deposition mechanisms taking place on the superheater tubes simultaneously.

On the wind side of the superheater tubes, facing the flue gas stream directly, larger particles depositing via inertial impaction contribute the most to the deposit build-up. The larger particles can reach diameters of up to a few millimetres and are partially or fully molten. [10] They originate from partially burned black liquor droplets, entrained in the flue gas stream. Thus, these larger particles contain typically sodium-sulfate and -carbonate.

On the lee side of the superheater tubes fine fume particles deposit via thermophoresis or eddy impaction. These fume particles are of submicron size and form in flight as the inorganics that have been vaporized during combustion condense while travelling along the flue-gas path and the local temperature decreases. Fume particles consist mainly of sodium sulfate but contain also chlorine. [9]

A third deposit formation mechanism is direct condensation of alkali vapours from the flue gas on the steel surface.[11] It is commonly agreed on that this is the first step in the deposit formation process, as the thin layer of condensed alkali salts (predominantly chloride) creates a sticky surface on the superheater tube, which then makes deposition via the above-mentioned mechanisms easier and the deposit starts to grow on the superheater tubes.[1]

As the deposit grows on the superheater tubes, a temperature gradient builds up along the cross-section with the local temperature being the coldest at the steel surface and increasing with distance from the steel, towards the hot flue gas. A schematic of such a temperature gradient is shown in Figure 3.

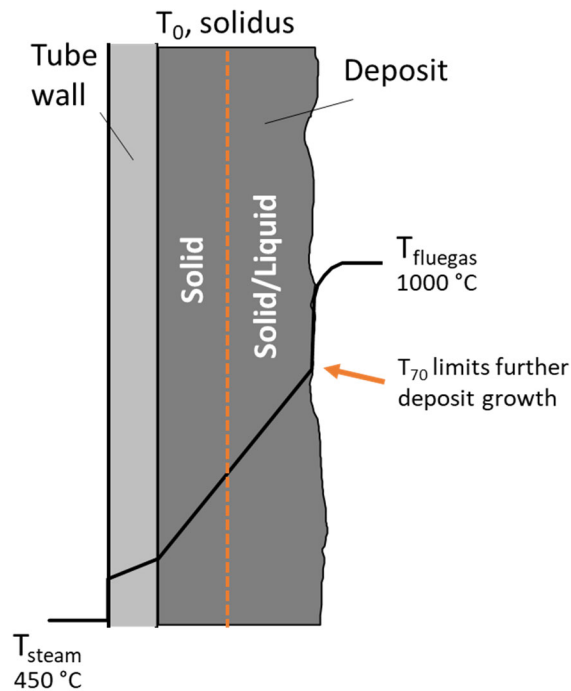


Figure 3: Temperature gradient over a superheater deposit during boiler operation [12]

The solid part of the deposit indicated in Figure 3 is in practice porous while the part of the deposit at temperatures above T_0 can form a dense non-porous layer as the formed melt fills the pores between single particles of the deposit, depending on the amount of melt present.

The schematic in Figure 3 depicts already one vital part of research connected to ash deposit chemistry, which is to avoid T_0 from reaching the steel surface to avoid severe melt-induced corrosion. Advanced knowledge of the deposit composition, thus its melting behaviour is essential to achieve this goal. But as several deposition mechanisms contribute to the overall deposit build-up simultaneously, the local composition of the deposit can differ from the bulk composition, which can result in local differences in the melting behaviour of deposits.

These local changes in deposit composition have been identified in several full-scale deposit measurements.[8,13–15] The first time local differences in the deposits chemical composition have been reported has been on probe measurements carried out by Reeve et al.[16] where deposits were collected using air-cooled probes. Depending on the local temperature, differences in the deposits chloride and potassium content have been identified, with the highest amounts of both compounds being located close or at the probe surface. It has been concluded by Reeve et al. that the observed differences are connected to the different deposition mechanisms contributing to deposit build-up but also partly to intradepositional processes taking place after deposition. More recently, Costa et al.[14] have shown differences within the deposit composition along the cross-section, with Cl and K being enriched toward the steel. The enrichment in these elements observed by Costa corresponds to locally lower T_0 inside the deposit, enabling melt formation directly at the steel surface and resulting in severe corrosion of the superheater tubes. Costa et al have concluded that a combination of predominantly condensing alkali chloride in the early phase of deposit build-up, but also diffusional transport processes through the deposit have been responsible for the observed local enrichment.

The objective of the present work is to better understand changes in deposit chemistry due to the temperature gradient as a function of time. These changes take place after the initial deposit formation and will be referred to as deposit ageing in the further course of this report. Identifying and

understanding the underlying mechanisms responsible for local changes within the deposit chemistry is of great importance when predicting a deposit's melting behaviour and morphology, thus being able to estimate the corrosiveness and also the removability of deposits. Several of such mechanisms could be identified and studied thoroughly on a laboratory scale, under well-controlled conditions,[12,17–20] but data on actual kraft recovery boiler superheater deposits are scarce. A further goal of the current research is to confirm laboratory test results using full-scale data.

Identification of mechanisms that change deposit morphology and chemistry over time

Laboratory set-up used to study deposit ageing

Motivated by the above-mentioned studies, deposit ageing and the effect of a temperature gradient on superheater deposits have been studied more extensively at Åbo Akademi University. Photographs of the custom design experimental set-up that has been used to study the effect of a temperature gradient on synthetic ash deposits of various compositions over time are shown in Figure 4. [12]

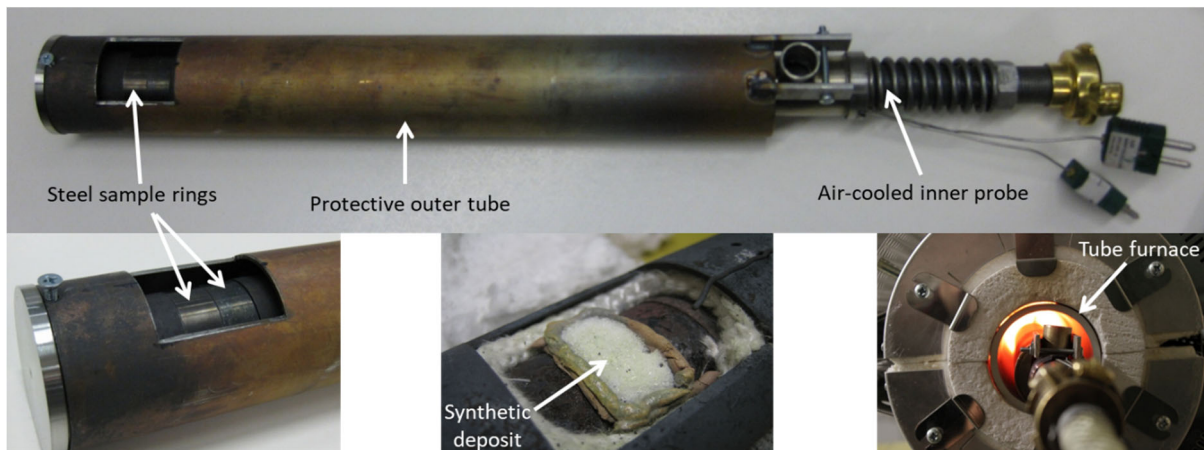


Figure 4: Experimental set-up to study deposit ageing mechanisms on laboratory scale [19]

The probe consists of two concentric tubes. The inner tube can be equipped with two steel sample rings. On top of these rings, a synthetic deposit is placed. As the experimental conditions reach temperatures above the first melting point of the deposits, a mould of heat-resistant paste is placed around the synthetic deposit to avoid it from flowing off the steel sample ring. The inner tube is air-cooled and two thermocouples are placed inside the steel rings to control and log the steel temperature constantly over the whole experimental duration. During the experiment, the probe is placed inside a tube furnace. The outer tube is used for thermal insulation purposes as it reduces additional cooling effects emanating from the probe toward the furnace and thus ensures more stable temperatures during the experiment. As the temperature of the tube furnace and the steel sample rings can be regulated separately, a temperature gradient can build up between the cool steel ring and the hot furnace. A schematic of the experimental setup including measured temperatures is shown in Figure 5. [12,19]

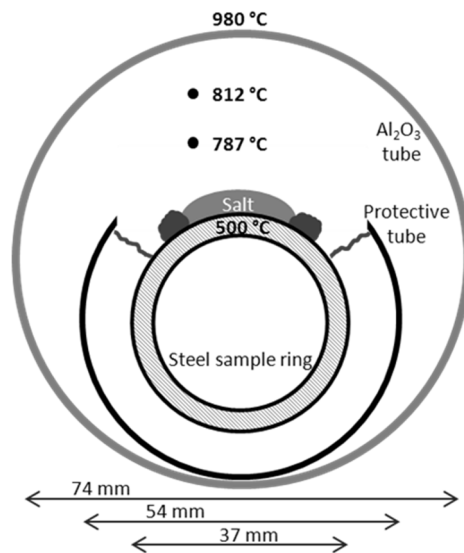


Figure 5: Schematic cross-section of laboratory set-up depicting the temperature profile between the cool steel sample ring and the hot furnace [19]

The advantages of the laboratory setup are good reproducibility, well-controlled experimental conditions, and the possibility to study deposit ageing mechanisms systematically.

After termination of an experiment, the steel sample rings are removed from the probe, with the aged deposit still attached to the steel. The obtained samples are subsequently cast in epoxy resin and cut to obtain a cross-section. The cut samples are then polished, carbon-coated, and analysed using scanning electron microscopy and energy dispersive X-ray analysis (SEM/EDX).

Synthetic deposits of varying chemical compositions have been studied using the described experimental set-up. The synthetic deposits consist usually of Na, K, Cl, SO₄. In the early stages, binary mixtures containing mixtures of NaCl-Na₂SO₄ or KCl-K₂SO₄ were mainly utilized, but later on, more complex salt mixtures were studied as well, by adding the respectively missing alkali metal compound. The increased complexity of the synthetic salt mixtures has also been a step toward compositions more accurately representing actual kraft recovery boiler superheater deposits.

Deposit cross-sections obtained from the laboratory tests varied in their appearance as a result of the varying composition of the used synthetic salt mixture. In Figure 6, SEM images of cross-sections of several deposits can be seen.

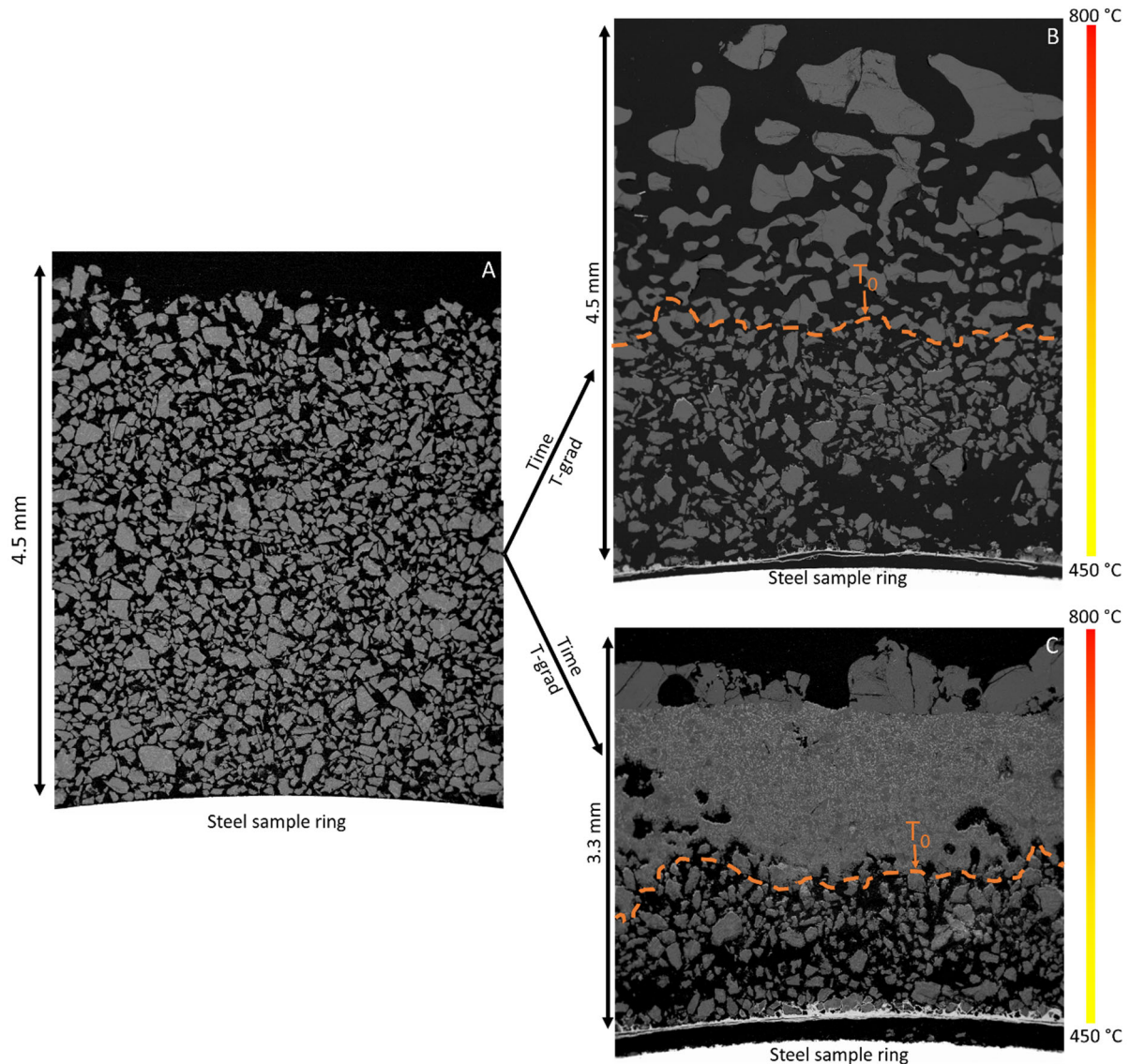


Figure 6: SEM cross-sectional images of synthetic ash deposits A) Before exposure to a temperature gradient, B) and C) After exposure to a temperature gradient

All the cross-sectional images in Figure 6 are oriented in the same way, meaning that the steel surface to which the deposit is attached is located at the bottom of the image. The same orientation will be applied to all following SEM images in this report unless explicitly stated otherwise. This also implies that the local temperature within the deposit increases in the vertical direction with temperatures being the lowest on the bottom of the image, close to the steel, and increasing toward the upper edge of the deposit.

Image A in Figure 6 shows a synthetic deposit before exposure to a temperature gradient. The deposit consists of distinct particles of irregular shape. The particle size for all laboratory experiments has been chosen to be in the range between 53 μm to 250 μm .

Images B and C of Figure 6 show two deposits after exposure to the temperature gradient. The morphological differences between the deposits in images B and C are due to differences in their chemical bulk composition.

Based on the morphological structure of the deposits, the location of T_0 within the cross-sections, at the time the experiment has been ended, can be located. In Image B the deposit particles start to fuse at a certain distance from the steel, resulting in larger agglomerates. Furthermore, the edges of the formed agglomerates are more round compared to the particles in image A, before exposure to the temperature gradient. Thus the border between partially molten (above T_0) and unmolten particles (below T_0) is expected to be located at the transition point of the two described morphologies.

The morphology of Image C in Figure 6 differs significantly from that in Image B. The differences are caused by the higher Cl content in the synthetic salt utilized in image C. As pointed out previously, the amount of melt formed within a deposit is closely linked to its Cl content. The higher amount of melt present within deposit C results in the formation of the observed dense layer at higher local temperatures. The amount of melt formed within the deposit is sufficient to fill the pores between the original particles which results in the formation of the dense layer on the outer part of the deposit.

The location of T_0 within a deposit of the type shown in image C can also be determined based on its morphology. The interface between the dense molten layer and the porous region underneath depicts the location of T_0 .

The above-presented laboratory setup proved to be a particularly suitable tool to study deposit ageing mechanisms on a laboratory scale. Three deposit ageing mechanisms have been identified and characterized using the laboratory setup. Figure 7 gives a summary of the deposit ageing mechanisms identified using the laboratory setup.

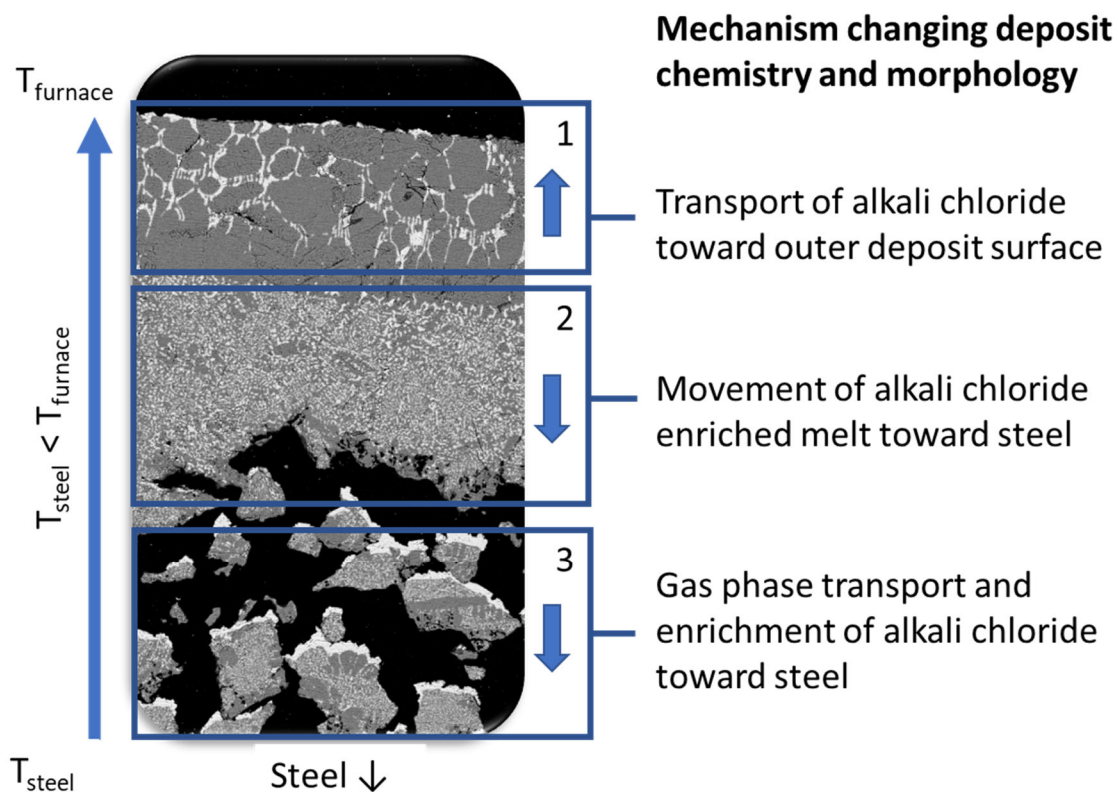


Figure 7: Main aging mechanisms identified in laboratory experiments using synthetic ash deposits

All deposit ageing mechanisms that have been identified are connected to intra-deposit transport phenomena of alkali chloride. The three deposit ageing mechanisms indicated in Figure 7 will be presented in more detail within the next paragraphs.

Temperature gradient zone melting

Within section 1 in Figure 7, the outermost region of the deposit, channels of alkali chloride can be seen (white colour in SEM image). Over time, the alkali chloride within these channels moves toward the outer surface of the deposit where it then subsequently evaporates into the furnace due to the high local temperatures on the outer deposit surface. The evaporation from the deposit outer surface takes place in laboratory conditions, whereas in boiler conditions the flue gas can be expected to contain some concentration of alkali chloride in gas phase, limiting the evaporation from the deposit into the flue gas. The mechanism responsible for the formation of the channels of alkali chlorides has been identified to be temperature gradient induced [17] and behaves similar to a mechanism called temperature gradient zone melting, which is well known in geological and metallurgical processes [21–24] but has not been identified in connection with ash deposits before.

Ash deposits melt over a larger temperature range, and the composition of the formed melt is temperature-dependent. Therefore, the local composition of the melt within a deposit varies locally and can be described as a function of distance from the steel due to the temperature gradient. A schematic overview of the mechanism is shown in Figure 8 on the example of the NaBr – Na₂SO₄ system.[18] The Br can be replaced by Cl in this example without affecting the basic principles of the mechanism.

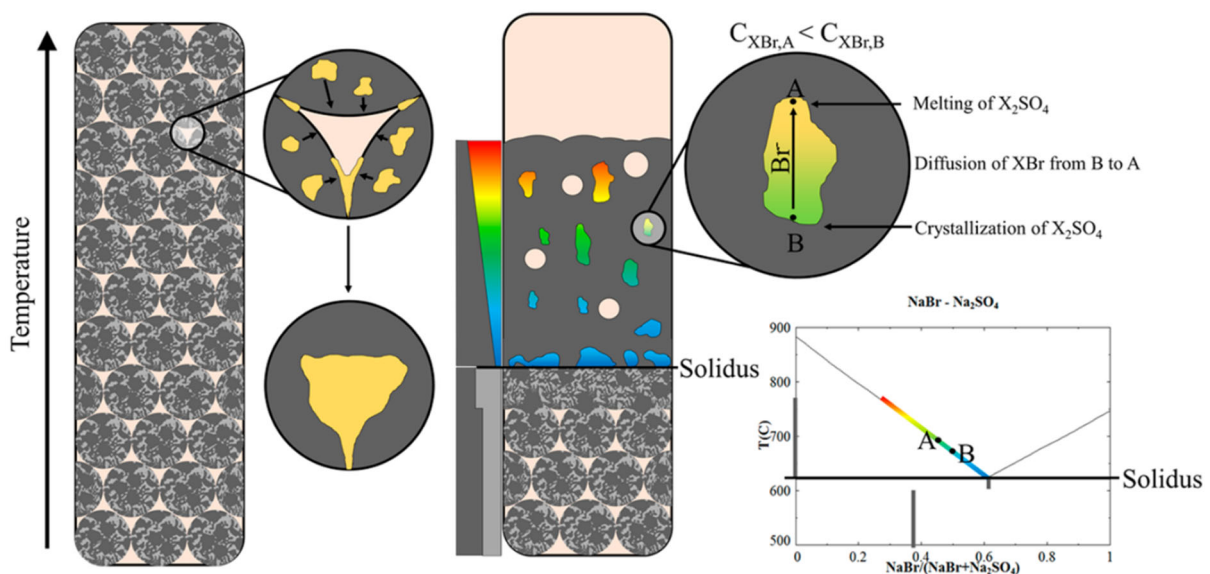


Figure 8: Schematic of temperature gradient zone melting in synthetic ash deposit of NaBr-Na₂SO₄ system

As the porous deposit starts to melt, the formed melt accumulates in the pores of the original deposit and forms droplets. Due to the temperature gradient over the deposit, the composition of the melt within these droplets can vary locally. Furthermore, the phase diagram in Figure 8 shows that all alkali bromide will be in molten state at temperatures above T_0 together with a varying share of alkali sulfate. The remaining solid phase consists of pure alkali sulfate. At the colder side of the melt droplet, the alkali halide concentration in the melt is lower compared to the hotter end of the droplet. This concentration gradient within the melt initiates diffusional transport processes of alkali halide from the cooler region (higher halide concentration) to the hotter region (lower halide concentration) within a melt droplet. As a consequence of this diffusional transport within the melt, the local concentration of SO₄ increases at the colder end of the melt droplet, resulting in solidification of alkali sulfate while simultaneously, the SO₄ concentration at the hotter side of the melt droplet decreases which initiates dissolution of alkali sulfate from the surrounding solid phase. This process of continuous diffusional transport of alkali halide in combination with solidification at the cool end and dissolution at the hot

end of the melt droplet results in a net effect of melt moving through the solid phase away from the steel, toward the outer deposit surface. As the melt reaches the outer deposit surface, the alkali halide evaporates into the furnace, leaving behind a region of the deposit depleted in alkali halide consisting of pure alkali sulfate. The SEM images in Figure 9 show the gradual progress of the process of temperature gradient zone melting.[18]

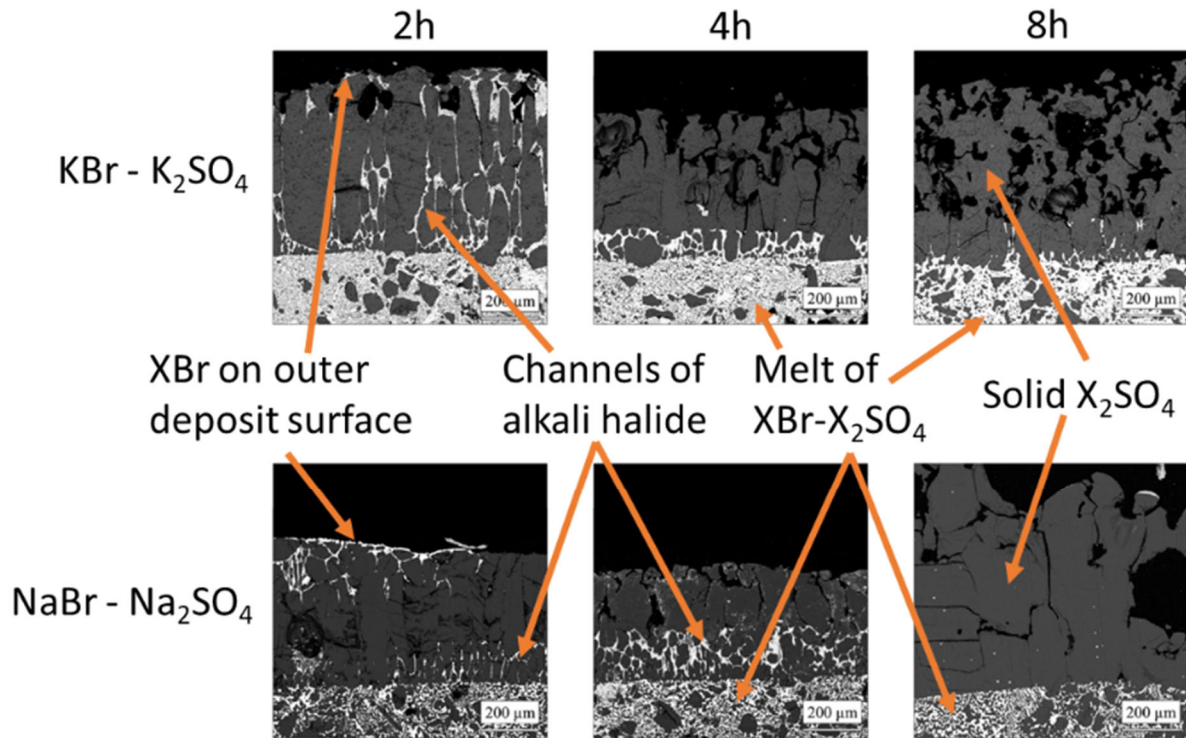


Figure 9: SEM images depicting different stages of temperature gradient zone melting within synthetic ash deposits containing XBr-X₂SO₄

From the SEM images of the synthetic deposits shown in Figure 9, it can be seen that the mechanism takes place already during the early stages of deposit melting as a layer of melt could be seen already after an exposure time of 2 hours on the outer surface of the deposit. After 8 hours, the outer deposit surface consists of a dense layer of alkali sulfate. The mechanism of temperature gradient zone melting is expected to increase the deposit density, which can impede deposit removability.

Movement and enrichment of melt toward the steel

In section 2 of Figure 7 melt enriched in alkali chloride can be seen. The laboratory experiments have shown that this melt moves toward the colder steel surface over time. The driving factors for the observed melt movement toward the steel surface have been identified to be capillary and gravitational forces.[19]

As larger amounts of melt form within the deposit at local temperatures above T_0 , the melt starts to fill the pores as already described in the previous chapter. But as the amount of melt formed increases, the gravitational and capillary forces grow, resulting in movement of melt toward the colder steel surface. As the melt gets transported toward the steel, the local temperature within the deposit decreases. This decrease in local temperature results in partial solidification of the melt until the local temperature of T_0 is reached and the melt is fully solidified.

If the steel temperature is set too high, the melt can get into direct contact with the steel surface, which can result in severe corrosion of the superheater steels.

Furthermore, laboratory experiments have shown enrichment of Cl and K in the melt toward the steel. This enrichment can result in local changes of the first melting / final solidification temperature (T_0), increasing the risk for melt-induced corrosion. Differences in T_0 locally within the deposit means that the first melting point of the deposit is not constant, based on its average bulk composition but can vary due to local changes of the deposit chemical composition. Local changes in T_0 enable presence of melt at temperatures lower than the first melting temperature of the bulk deposit, thus increasing the risk for melt-induced corrosion of superheater surfaces.

In kraft recovery boilers, the molar ratios of chlorine to total alkali ($Cl/(Na+K)$) and potassium to total alkali ($K/(Na+K)$) are commonly used indicators to assess the corrosiveness of deposits. These ratios have been calculated for the synthetic ash deposits analysed in the laboratory studies. In Figure 10, the average $K/(Na+K)$ and $Cl/(Na+K)$ ratios as function of distance from the steel are shown.

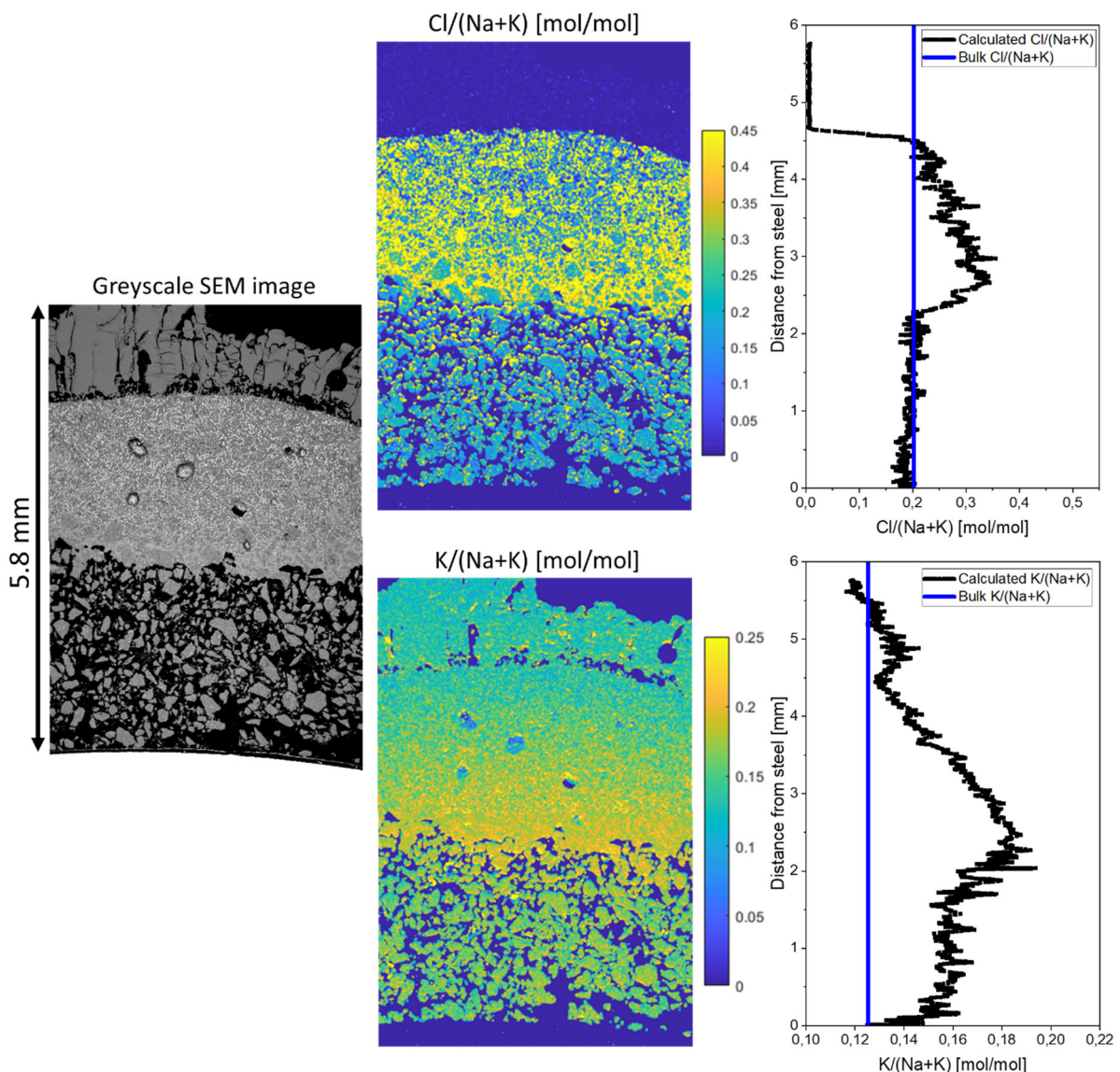


Figure 10: Cl and K distribution within a synthetic ash deposit based on molar $K/(Na+K)$ and $Cl/(Na+K)$ ratios

The cross-section shown in Figure 10 has a general deposit structure similar to that in Figure 7. The outer region, furthest away from the steel surface is depleted in Cl resulting in $Cl/(Na+K)$ ratios approximating values of 0. The K concentration within the Cl depleted region does not show a significant deviation from the bulk deposit composition.

On the one hand, the Cl depletion in the outer deposit region is caused by temperature gradient zone melting. On the other hand, melt formed on the outer deposit surface moves toward the steel surface resulting in enrichment of Cl and K toward the steel. As shown in Figure 10, the dense layer of the deposit, between the porous region close to the steel and the Cl depleted region on the outer surface is enriched in both Cl and K compared to the bulk deposit. The Cl and K concentrations show maxima at the interface between the porous and dense deposit regions. As reference, the $K/(Na+K)$ and $Cl/(Na+K)$ ratios of the original synthetic deposit (before furnace exposure) are shown in the graphs as vertical lines.

The observed enrichment is caused by partial solidification of the melt as it moves toward the steel surface and the local temperature decreases. As a result of lower local temperatures, the melt starts to solidify partially. Thus the melt composition is not constant throughout the whole cross-section but can be described as a function of distance from the steel. This results in the observed concentration gradient for both Cl and K in the dense layer above the porous deposit region.

A direct consequence of the melt being enriched in Cl and more importantly K is the local change in the first melting temperature. To illustrate the effect of melt enrichment on the local first melting temperature, the cross-section shown in Figure 10 has been divided into several sections. For each of these sections, the average composition has been calculated based on the data obtained from SEM/EDX analysis. The first melting temperature of each section could then be calculated using the thermodynamic software FactSage version 7.3 and the FTPulp thermodynamic database, relevant for alkali salts in kraft recovery boiler conditions.[25] The respective sections and the corresponding local values for T_0 are shown in Figure 11.

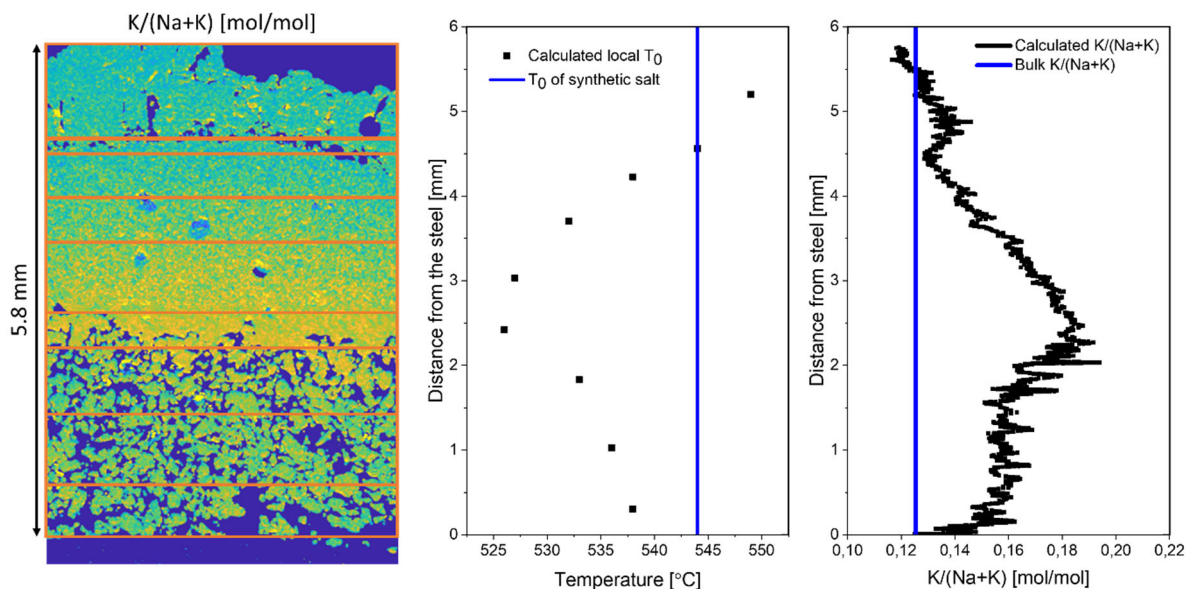


Figure 11: Segmented SEM cross-section of synthetic deposit and respective local T_0 values

The T_0 profile shown in Figure 11 indicates a correlation between the local T_0 value and the K content within the deposit. As already mentioned above, the K content in a deposit affects the first melting temperature. Due to solidification, K is enriched in the remaining melt, resulting in higher local concentrations of K toward the steel which then in turn lowers the local first melting temperature. The deposit reaches a minimum in the local first melting temperature at the interface between the porous region and the dense molten layer where the local K concentration within the deposit is the highest.

The results imply that not only knowledge of the initial deposit composition is required when assessing the corrosiveness and the first melting temperature of a deposit, but due to deposit ageing

mechanisms, the local first melting temperature can reach values lower than those of the original bulk deposit composition. If these local changes in the deposits first melting temperature are not accounted for, the steel temperature in boilers might be chosen too high in the hottest superheaters, and melt induced corrosion might occur in these regions of a boiler, despite T_0 calculations based on the deposit bulk composition implying the formation of melt does not occur at that temperature.

Gas-phase transport of alkali chloride

In section three of the deposit in Figure 7, the local temperature did not reach values above T_0 . The deposit remained in its original morphology of distinct irregularly shaped particles. Within this porous region, formation of pure alkali chloride layers on the furnace facing side of the particles could be observed. These layers are formed as a consequence of diffusional transport of alkali chloride vapours toward colder temperatures within the porous region of the deposit.[12,17] Figure 12 describes the underlying mechanism resulting in the formation of the observed alkali chloride layers.

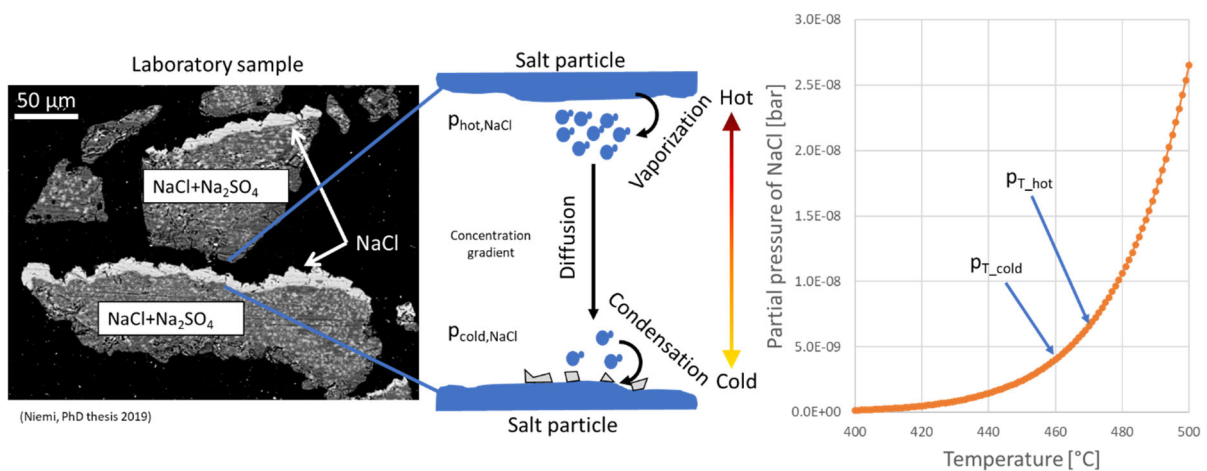


Figure 12: Alkali chloride gas phase transport mechanism in porous deposits [17]

Due to the temperature gradient, the deposit is exposed to, the temperatures on the outer surface of the single particles differ from one another. Again, the temperature can be described as a function of distance from the steel, where the local temperature increases with the distance from the steel. This results in a situation as shown in Figure 12

Of the two particles shown, the temperature on the top (furnace facing side) of the lower particle is lower compared to the surface temperature at the bottom (steel facing side) of the particle above. At temperatures present within the porous layer of the deposit, the formation of alkali chloride vapours is possible due to evaporation of alkali chloride from the solid particles. The partial pressure of alkali chlorides is temperature-dependent as shown in the graph to the right in Figure 12. This temperature dependence causes the build-up of a concentration gradient of alkali chloride vapours in the gas phase. As a result of the concentration gradient, diffusional transport of alkali chloride toward the cooler regions, thus of lower alkali chloride vapour concentrations, takes place. As the saturation pressure on top of the colder particle is reached, alkali chlorides start to condense on top of the particle surface. At the same time, more alkali chloride evaporates from the particle above, with higher local temperatures, resulting in particles being depleted in alkali chloride. This alkali chloride vapour transport is a continuous process and can go on until either the hotter particles are completely depleted in alkali chloride or the alkali chloride layer on the colder particle grows that thick so the gap between the single particles is closed.

This gas-phase transport of alkali chloride within the porous region of the deposit alters the deposit composition locally which can affect the local melting behaviour of deposits. In addition, corrosive

alkali chloride has been observed to condense directly on the steel surface [19] posing an increased risk for alkali chloride-induced corrosion.

Melting behaviour – impact of amount of melt on deposit morphology

As already mentioned above in Figure 6, the morphology of the deposits observed after exposure to the temperature gradient varied between samples. The morphological differences are connected to changes in the melting behaviour of the artificial deposits. It is currently assumed that not only T_0 and the amount of melt formed at T_0 are crucial parameters when talking about deposit chemistry and the melting behaviour, but also the amount of melt present at the outer deposit surface. A certain amount of melt is required for extensive liquid phase sintering to take place and pore filling mechanisms to start, which then results in the formation of the dense molten layer toward the outer, hot deposit surface. Thus all cross-sections analysed so far were categorized regarding their morphology, whether they formed a dense sintered layer (Image B in Figure 6) or a skeletal layer (Image C in Figure 6) on the outer deposit surface. Based on the chemical composition of the salt mixture and the measured temperature at the outer deposit surface during exposure to the temperature gradient, the amount of melt present at the outer deposit surface can be determined. In Figure 13 the observed morphology for all samples analysed thus far are summarised indicating the amount of melt present on the outer deposit surface during exposure.

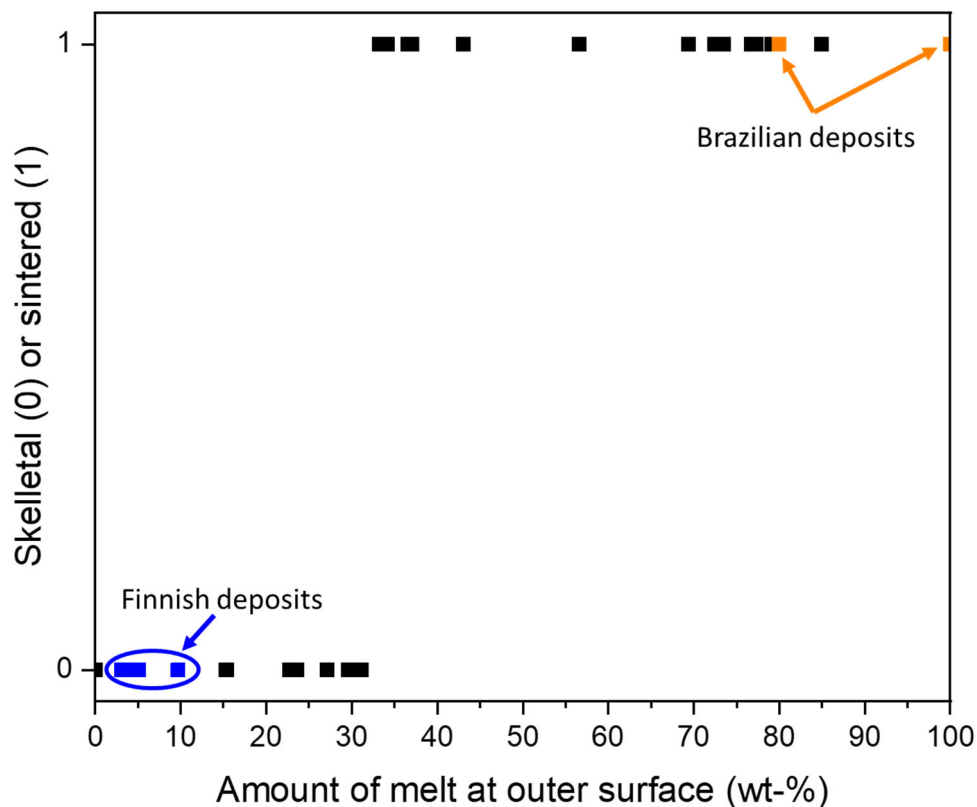


Figure 13: Impact of amount of melt formed at outer deposit surface on morphological structure of aged deposit

In addition to the artificial deposits, data from kraft recovery boiler superheater deposits are included in Figure 13 as well. The superheater deposits will be discussed separately later on in this report.

The data presented in Figure 13 implies that transition from a skeletal to sintered deposit morphology takes place at an amount of melt of approximately 35 wt-%.

Knowledge on which deposit morphology is to be expected helps in estimating which of the deposit aging mechanisms introduced above might be governing in the respective sample. Furthermore, the deposit morphology can influence the removability of the deposit as the more porous skeletal morphology is expected to be more brittle compared to the dense deposit morphology, thus skeletal deposits are easier to be removed via sootblowing.[26]

Kraft recovery boiler superheater deposits

In addition to the laboratory experiments, actual superheater deposits were obtained from two kraft recovery boilers. One recovery boiler is located in Belo Oriente, Brazil and the other boiler is located in Rauma, Finland. Schematic drawings of the superheater areas of the two boilers are shown in Figure 14

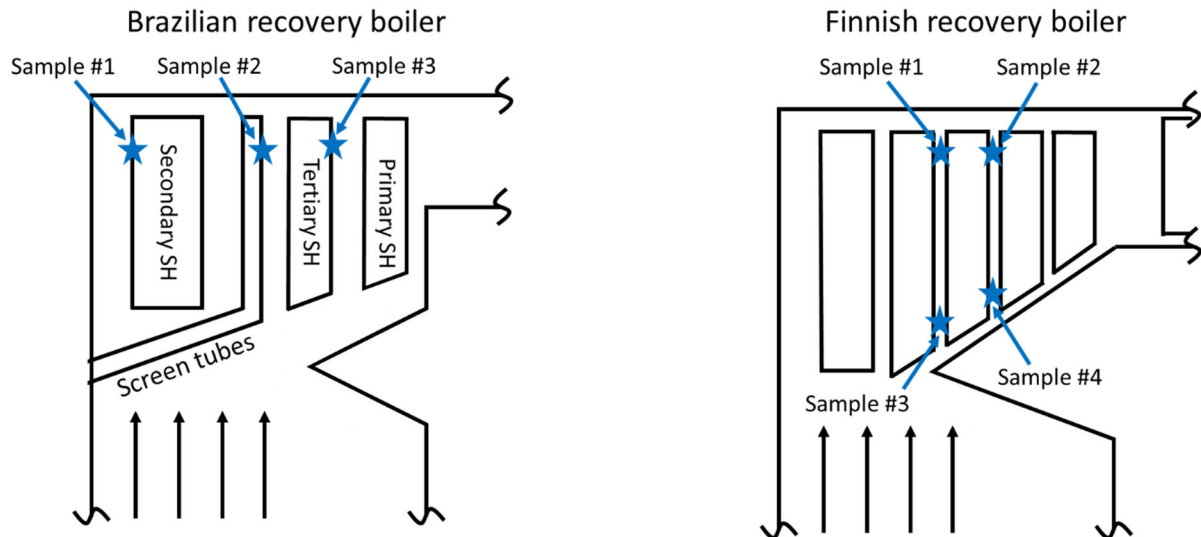


Figure 14: Schematic drawing of convective pass of Brazilian (left) and Finnish kraft recovery boiler (right) indicating locations of superheater deposit sampling

The sampling locations of the obtained deposits are indicated with stars. In the Brazilian boiler, deposits have been obtained from three different locations along the convective pass of the boiler, resulting in differences in the steel temperature between the samples. The Finnish superheater deposits have all been obtained from the tertiary superheater tubes but at varying locations.

In both boilers, the samples have been taken during a boiler shut-down. The superheaters have been accessed through inspection hatches in the boiler wall and the deposits have been removed from the superheater tubes they were attached to. Due to the used sampling method, it cannot be guaranteed that the innermost layers of the deposits have not been damaged or have been completely removed from the superheater tube during the sampling process.

Compared to the synthetic deposits presented in the previous chapter, the expected temperature gradients in superheater deposits are significantly smaller. While the calculated temperature gradients in the laboratory samples ranged on average between 60 to 100 °C/mm, temperature gradients in actual boiler deposits are expected to be in the range of 10 °C/mm. These differences in the magnitude of the temperature gradients can be expected to affect the speed of temperature gradient-induced deposit ageing processes within the actual superheater deposits when compared to the laboratory samples using synthetic ash deposits. These differences in the temperature gradient between laboratory and full-scale deposits are caused by the deposit thickness as well as differences in furnace/gas temperatures. The full-scale superheater deposits are significantly thicker compared to the laboratory samples. Steel temperatures in laboratory experiments are typically chosen similar to the boiler steel temperatures of the hottest superheater. In laboratory, the furnace temperature can be chosen, but typically used temperatures in laboratory experiments are higher than the flue gas temperatures in the region of a boiler's hottest superheater.

Besides the differences in the temperature gradients, also the chemical composition of the superheater deposits differs from that of the synthetic deposits used in the laboratory experiments.

The main difference between laboratory and full-scale deposits is the presence of carbonate in the actual superheater deposits, whereas no carbonate is included in laboratory deposits due to the carbonate interacting with the paste holding the synthetic deposit in place in laboratory experiments.

There are differences in chemical composition when comparing the deposits obtained from the two boilers. In the Brazilian boiler, eucalyptus is utilized for the pulping process. In Finland typically spruce and pine are utilized. Thus, the black liquor composition hence the deposit composition differs between Nordic and South American kraft recovery boilers. Deposits obtained from the Brazilian recovery boiler have higher Cl concentrations compared to the Finnish deposits as the Cl content in liquors originating from eucalyptus is up to ten times higher than in spruce or pine wood liquor.[27] Average deposit compositions for samples from both recovery boilers are summarized in Table 1.

Table 1: Average chemical composition of superheater deposits obtained from Brazilian and Finnish kraft recovery boiler

Compound [wt-%]	Brazilian deposits	Finnish deposits
Na	34.4	31.6
K	3.4	4.9
Cl	4.4	0.7
SO ₄	37.5	48.9
CO ₃	20.3	13.9

Besides the differences in the Cl content, the Brazilian deposits have a higher carbonate concentration compared to the Finnish deposits. This difference is most likely connected to the sampling locations the deposits were obtained from. The Brazilian deposit Samples #1 and #2 have been taken at the entrance to the convective pass of the boiler, while the Finnish deposits have all been sampled at the tertiary superheater tube. The probability for carry-over particles that contain higher amounts of carbon depositing on the superheater tubes is higher at the entrance to the convective pass of the boiler, thus the carbonate content is expected to be higher in the Brazilian deposits as the composition presented in Table 1 is an average value based on all deposits obtained during the sampling campaign.

Similar to the laboratory experiments presented above, the superheater deposits obtained from the kraft recovery boilers gave new insights into deposit ageing mechanisms. The results will be presented in the following two chapters starting with the deposits obtained from the Brazilian kraft recovery boiler and followed by the Finnish superheater deposits.

Brazilian superheater deposits

All deposits obtained from the Brazilian kraft recovery boiler have had similar morphological features. The main part of the deposit has been of a dense morphology, indicating the presence of melt during boiler operation. Closest to the steel, a thin layer of distinct particles has been found for two of the three samples. Several deposit ageing mechanisms could be identified within the deposits and are exemplary illustrated based on the SEM cross-sectional image shown in Figure 15.

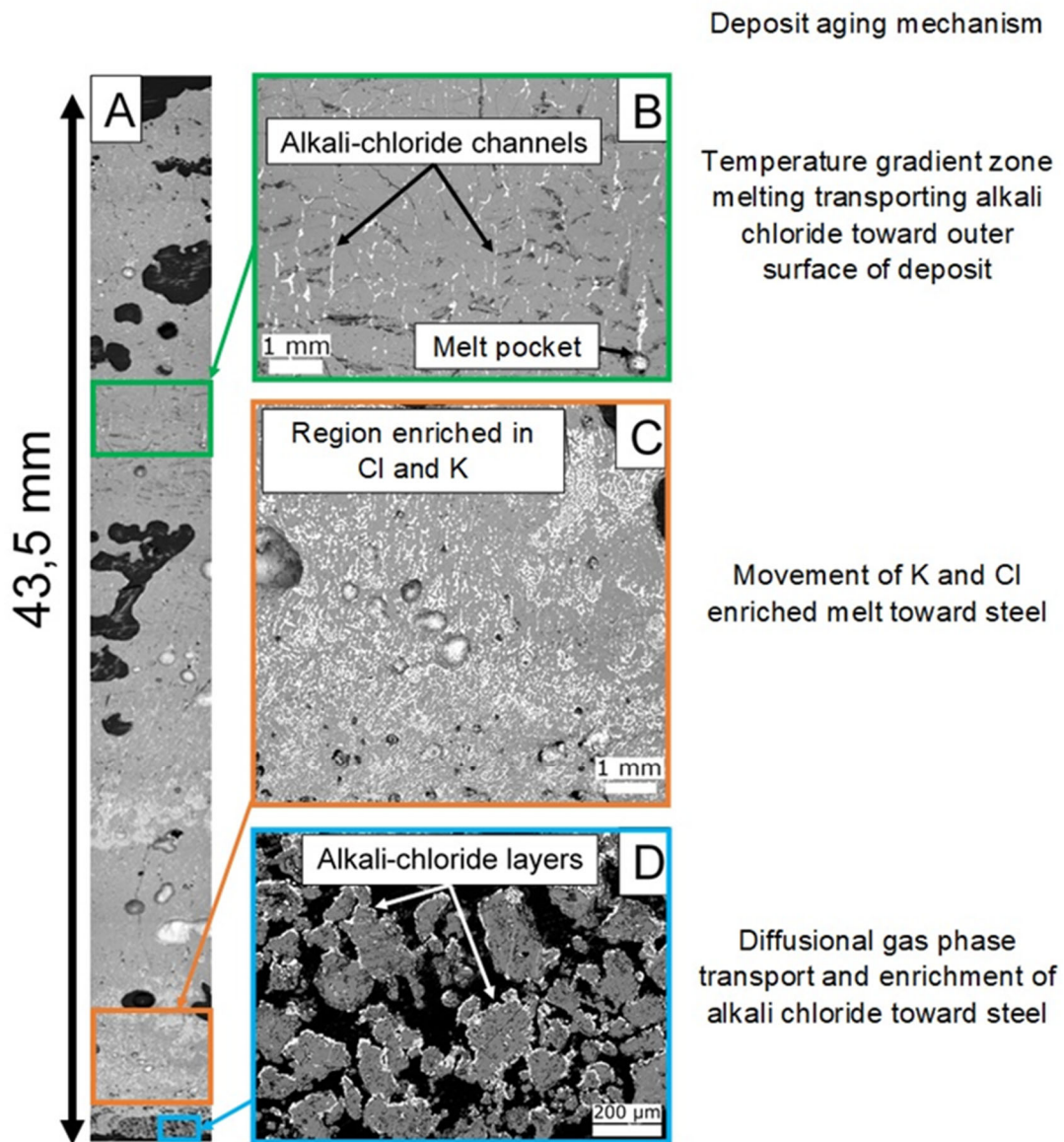


Figure 15: SEM image of cross-section of Brazilian superheater deposit indicating the main deposit ageing mechanisms [15]

As indicated in Figure 15, all three deposit ageing mechanisms which have been explained in more detail above could be identified within the Brazilian superheater deposits.

Closest to the steel, within the porous region of the deposit (Figure 15 D), alkali chloride layers could be identified. As the deposits have been removed from the superheater steel during analysis, it is not known to which extent Cl layers also have been formed directly on the superheater steel.

With increasing distance from the steel, the deposit morphology changes from porous to dense. The dense layer accounts for the bulk of the deposit. Throughout the dense deposit layer, channels of alkali chloride have been observed (Figure 15 B). It is expected that these observed channels have formed via temperature gradient zone melting, previously observed in the laboratory experiments using synthetic ash deposits.

Right above the porous region (Figure 15 C), a layer enriched in Cl and K could be observed within the samples. It is expected that the observed enrichment in K and Cl is a result of enriched melt being transported toward the steel. While the Cl concentration was fairly constant throughout the whole enriched region, a concentration gradient developed for K with the highest potassium concentration

at the interface between the dense layer and the porous region of the deposit. Melt enrichment resulting in a similar concentration gradient has been observed in laboratory experiments using synthetic ash deposits, which caused a local decrease in the first melting temperature of the deposit.

To evaluate the impact of the observed K enrichment toward the steel on the melting behaviour of the deposit, the SEM image of the cross-section has been divided into several sections, similar to the synthetic laboratory deposits. For each section, the average composition and the consequential first melting temperature have been calculated based on the elemental maps generated by SEM analysis. The results of the analysis of the local first melting temperature are shown in Figure 16 together with the elemental map of the K to total alkali ratio.

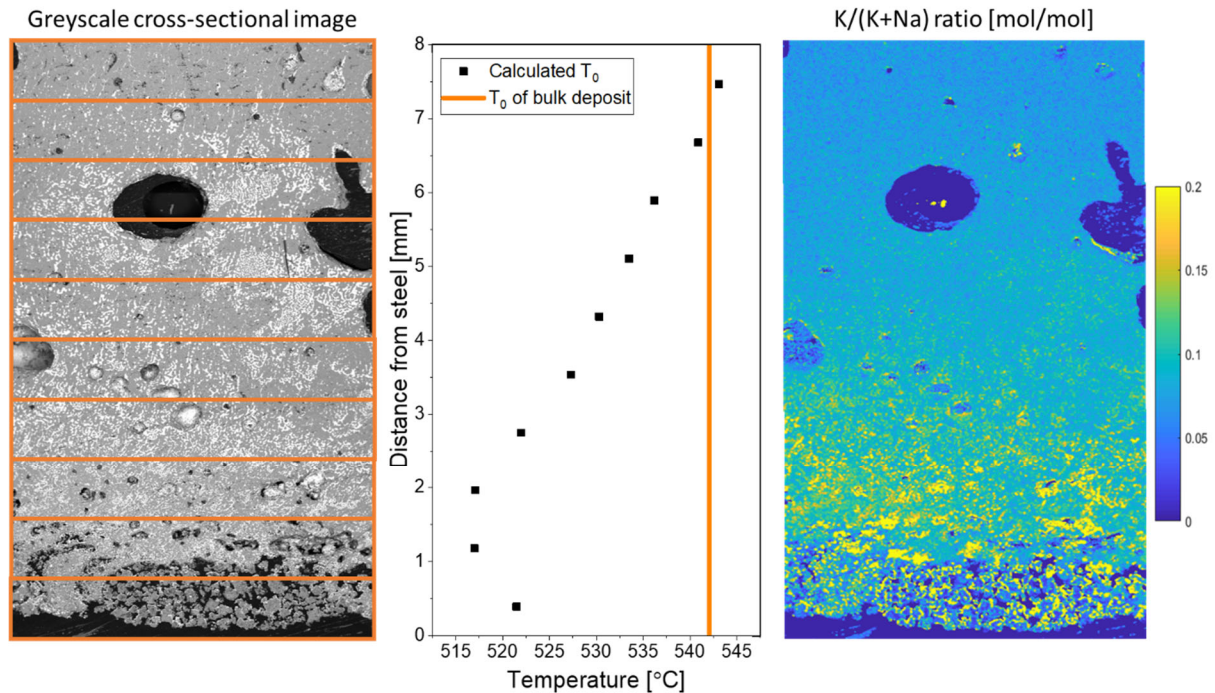


Figure 16: Impact of K enrichment toward the steel on the local first melting temperature in the Brazilian deposit [15]

As shown in Figure 16, the first melting temperature is not constant within the deposit, but decreases with increasing K concentration. The lowest local first melting temperature is located at the interface between the dense deposit morphology and the porous region of the deposit. At this interface, a maximum in the K concentration has been measured. The calculated local first melting temperature at this interface is significantly lower than that of the average bulk composition of the deposit and approaches the global first melting temperature of the K-Na-Cl-SO₄-CO₃ system at about 505 °C. A more detailed analysis of the Brazilian superheater deposits can be found elsewhere.[15]

The results from the analysis of the Brazilian deposits gave new insights into the melting behaviour of aged deposits. The results of both the laboratory experiments using synthetic ash deposits and the deposits collected directly from the superheater tubes of the Brazilian recovery boiler suggest local changes of the deposit's first melting temperature due to movement of melt enriched in K and Cl toward the steel. The results indicate that the local first melting temperature within a region enriched in K and Cl can reach the global minimum of the chemical system. In practice, this would mean that melt can be present at temperatures significantly lower than that of the average bulk composition of the deposit, which would then result in unexpected corrosion in some cases. [14]

Finnish recovery boiler deposits

Besides the Brazilian samples, superheater deposits have been obtained from a Finnish kraft recovery boiler located in Rauma. Due to the lower Cl content in the Finnish deposits, the morphology lacked the dense layer toward hotter local temperatures within the deposit. Furthermore, the Finnish superheater deposits did not have a uniform deposit morphology throughout all samples but have shown some variations. Exemplary SEM images of deposit cross-sections are shown in Figure 17.

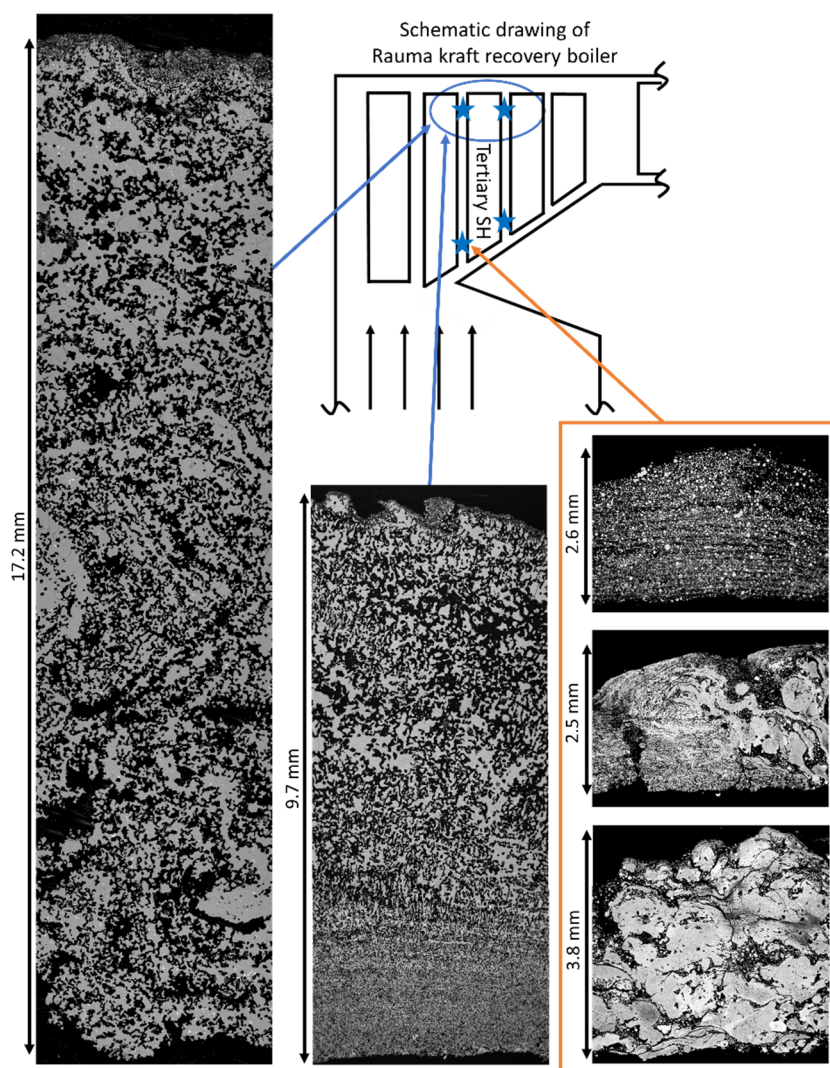


Figure 17: Cross-sectional SEM images of superheater deposits from Finnish kraft recovery boiler with varying morphology

Deposits obtained from the sampling locations close to the roof of the boiler appeared more structured. Deposits from the lower sampling locations, close to the bull-nose, had a larger variety in their morphologies. The larger variety is connected to the sampling location and the fluctuating conditions in the direction of the gas flow, due to the proximity to the bull-nose.

Due to the lack of a molten layer, the Finnish superheater deposits did not show enrichment of K and Cl through movement of melt. But instead, other observations connected to deposit ageing and local enrichment in K and Cl have been made. Two different enrichment patterns have been identified during the analysis of the Finnish superheater deposits.

Parallel enrichment of Cl and K (“Type 1” deposit)

Within some of the samples, local enrichment of K and Cl has been observed close to the steel. Based on the morphology of the deposits, the observed enrichment in Cl and K is expected to be caused by gas-phase transport of alkali chloride within the porous deposit structure.

Enrichment of Cl close to the steel has been observed in several samples. Layers of chlorine, parallel to the steel surface have been identified during elemental analysis. In the same region where the Cl enrichment has been observed, K enrichment occurred in the form of layers, parallel to the steel surface. In Figure 18 a “Type 1” superheater deposit with a region enriched in K and Cl at the same time is shown. In addition, the concentration profiles for both $K/(Na+K)$ and $Cl/(Na+K)$ are shown.

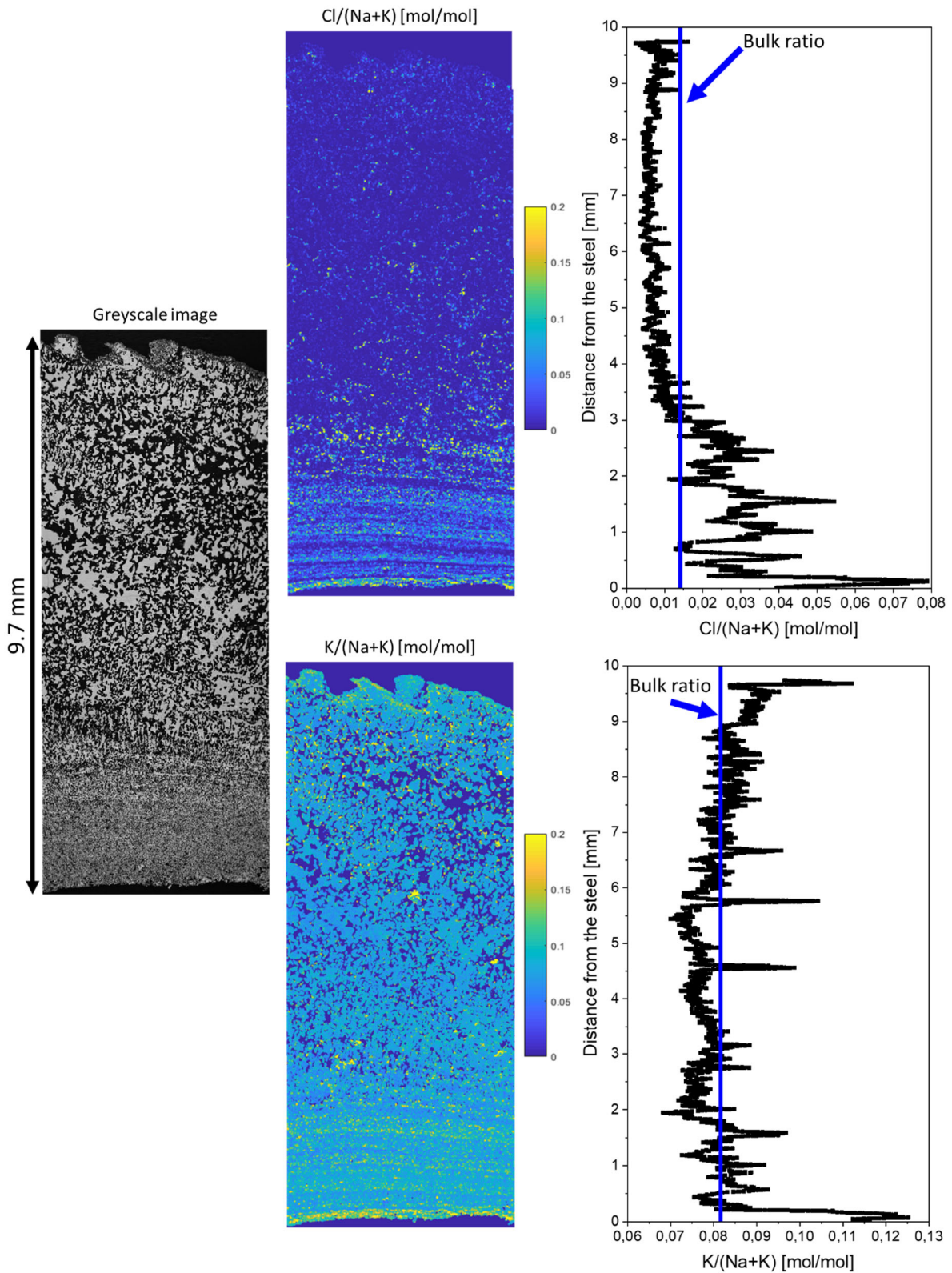


Figure 18: Finnish “type 1” superheater deposit with parallel layered K and Cl enrichment close to the steel surface

Due to the layered appearance of the enrichment within these deposits, the enrichment is expected to be connected to diffusional gas-phase transport of alkali chloride within the region closest to the steel. The layers of alkali chloride are difficult to detect in a grey-scale image, even at higher

magnifications. There are two main reasons for this difference compared to the laboratory samples. First, the Cl content of the Finnish superheater deposits is significantly lower compared to the Cl content of the synthetic deposits used in the laboratory experiments and the Brazilian superheater deposits. In addition, the local temperature gradient within superheater deposits is significantly lower compared to that in laboratory experiments, which is slowing down the diffusional transport rate.

Actual superheater deposits are thicker compared to the synthetic deposits studied in the laboratory setup. Furthermore, the flue-gas temperature within the region of the boiler where the samples have been taken from is lower compared to the temperature in the laboratory studies. In addition, the synthetic deposits in the laboratory experiments have formed a dense molten layer on the outside of the deposit, further away from the steel, which increases the thermal conductivity in that region and results in higher temperature gradients in the porous region located between the molten layer and the steel surface.[28] Thus, despite the significantly longer exposure time of the superheater deposits compared to the laboratory experiments, the actual thickness of the alkali chloride layers within the deposits are still very small.

Nevertheless, clear enrichment in Cl and K close to the steel has been observed and the effect of this enrichment on the local first melting temperature of the deposit has been analysed. To analyse the local melting behaviour the same procedure also used for the synthetic laboratory and Brazilian deposits has been used. The results of the calculations of the local first melting temperature are presented in Figure 19

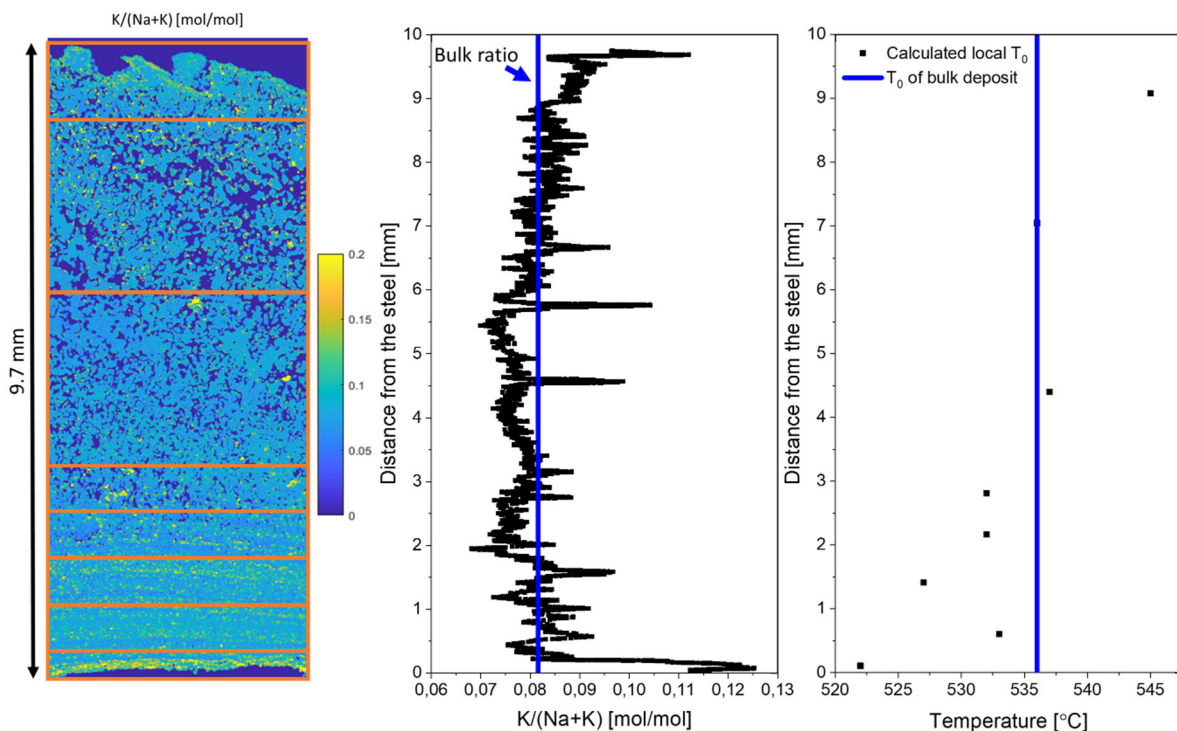


Figure 19: Local first melting temperature of Finnish "Type 1" superheater deposit

The results presented in Figure 19 show a decrease in the local first melting temperature throughout the whole K enriched region of the deposit, with a minimum in the region closest to the steel at the highest local K concentration. This implies that the local value of T_0 for the "Type 1" deposits from the Finnish kraft recovery boiler is strongly connected to the K concentration. Furthermore, deposit ageing mechanisms other than melt enrichment can result in a local increase in the K concentration and lower the local first melting temperature of the deposit significantly.

Separate enrichment in Cl and K ("Type 2" deposit)

The layered structure of alkali chloride close to the steel did not appear in all of the analyzed deposits that have been obtained from the Finnish kraft recovery boiler. In some deposits, a different structure could be observed in the region close to the steel. The innermost layer of the deposit, closest to the steel, has appeared to be enriched in K while being depleted in Cl. In addition, the K enriched region has shown enrichment in SO_4 . The region of the deposit above the K enriched region, further away from the steel, has shown enrichment of Cl without any significant depletion in K or SO_4 compared to the bulk deposit composition. Deposits with this described structure will be referred to as "Type 2" deposits in the following chapters of the present report. SEM images of a "Type 2" deposit with the described properties are shown in Figure 20 together with the graphs depicting the average molar $\text{Cl}/(\text{Na}+\text{K})$ and $\text{K}/(\text{Na}+\text{K})$ ratios and molar sulfate concentration.

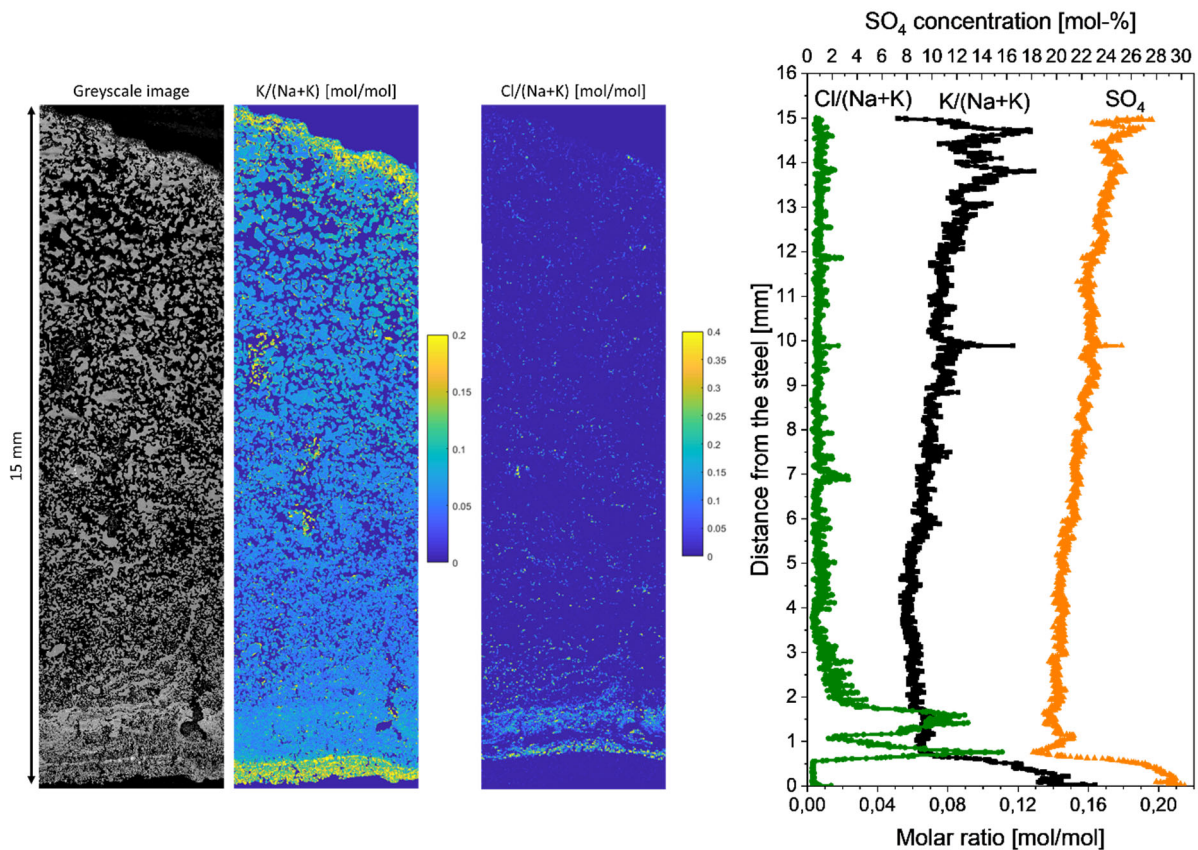


Figure 20: Greyscale, $\text{K}/(\text{Na}+\text{K})$, and $\text{Cl}/(\text{Na}+\text{K})$ SEM images of Finnish "Type 2" deposit and graphs of ratios together with molar SO_4 concentration

The depletion of Cl in combination with simultaneous SO_4 enrichment indicates sulfation of alkali chloride. During the sulfation reaction, gaseous SO_2 or SO_3 reacts with alkali chloride (NaCl or KCl) forming solid Na_2SO_4 or K_2SO_4 while HCl is released to the gas phase.[29] The local enrichment in SO_4 , close to the steel, indicates that the sulfation reaction takes place predominantly during the start-up phase of the boiler. Data on the SO_2 concentration in the flue gas stack could be obtained for the whole period the boiler was in operation prior to sampling (from start-up to shut-down). The SO_2 concentration in the flue gas stack for this timeframe is shown in Figure 21.

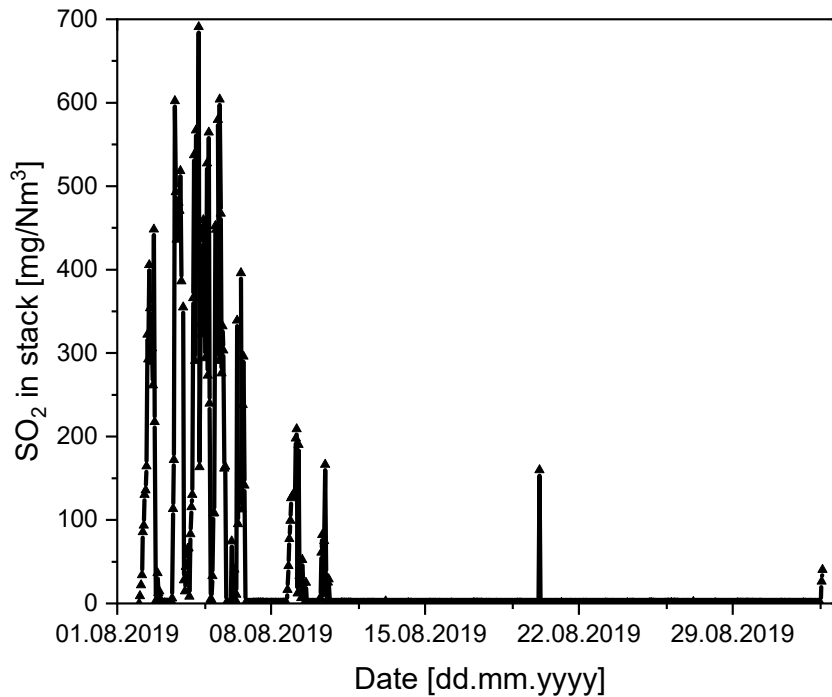


Figure 21: Measured SO₂ concentration in the flue gas stack during build-up period of Finnish superheater deposit samples

From the graph presented in Figure 21, it can be seen that the highest SO₂ concentrations in the flue gas stack are measured during boiler start-up. During start-up in this specific boiler, heavy fuel oil is used which typically results in higher SO₂ concentrations in the flue gas. After the startup phase, the SO₂ concentration is very low, with almost no SO₂ being present in the gas phase at all. The measured gas-phase concentration of SO₂ is in agreement with the high SO₄ content measured in the region of the deposit closest to the steel, which has been formed during the start-up phase of the boiler. This supports the proposed mechanism of sulfation of alkali chloride being responsible for the local enrichment in SO₄ within the deposit, closest to the steel.

To this point, it cannot be explained yet why a SO₄ rich layer is not present in all of the deposits that were analysed as part of this sampling campaign. A possible explanation might be an asymmetric furnace gas flow, that can result in local differences in the flue gas composition or temperature. Furthermore, the sulfation reaction of alkali chlorides does not explain the simultaneous enrichment in K in the SO₄ rich region shown in Figure 20. Currently, the observed K enrichment cannot be explained by any of the known deposit ageing mechanisms.

Similar to the deposits presented above, the impact of the observed enrichment on the local first melting temperature has been analysed for the “Type 2” deposits obtained from the Finnish recovery boiler. The results of the calculation are presented in Figure 22.

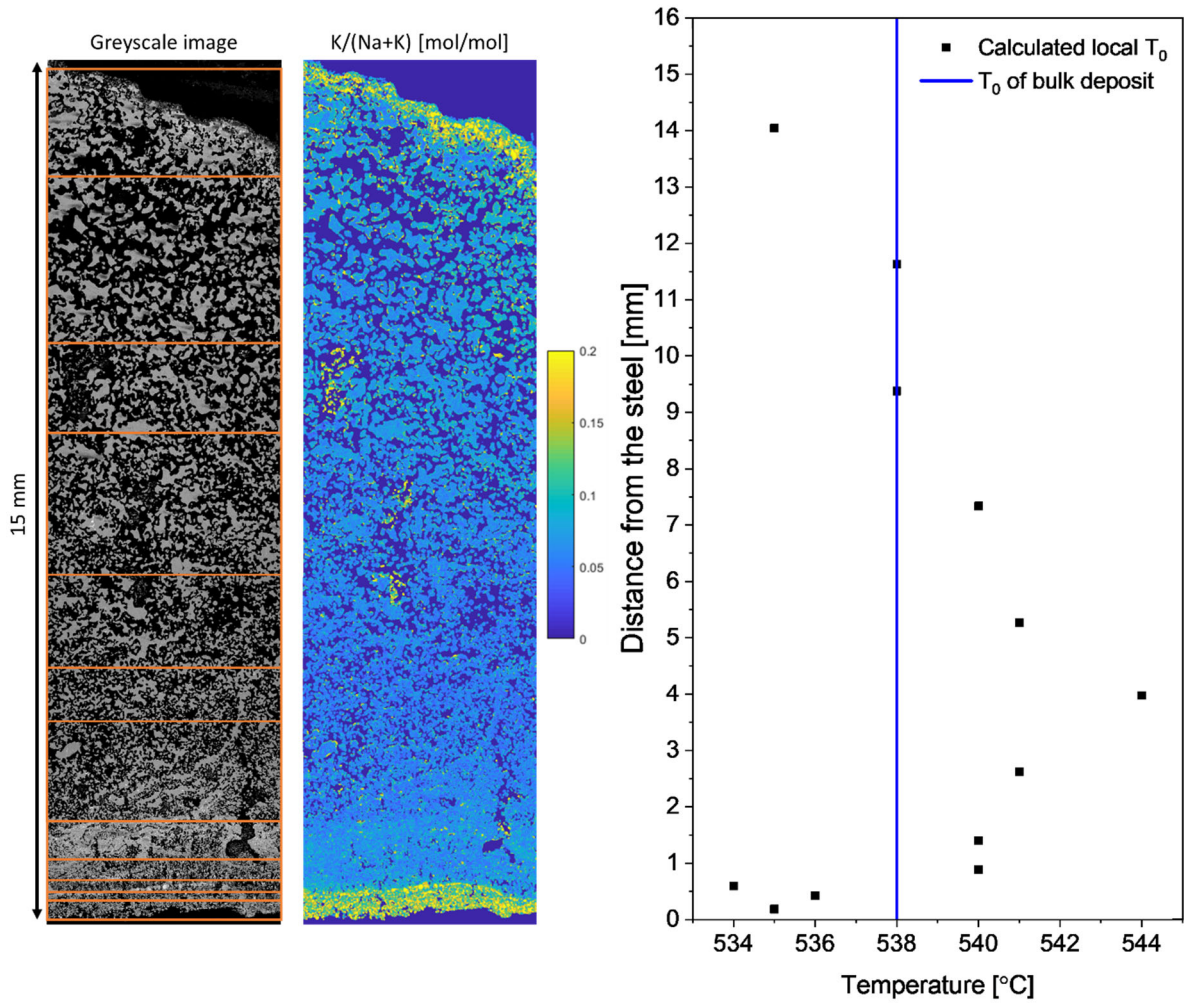


Figure 22: Local first melting temperature profile for Finnish "Type 2" deposit

Similar to the other deposit types presented above, the local first melting temperature of the "Type 2" deposit of the K enriched region closest to the steel is lower compared to that of the bulk deposit composition. This indicates that the local first melting temperature of the deposit decreases with increasing K content, regardless of the underlying enrichment mechanism.

Deposit ageing probe measurements in Rauma kraft recovery boiler

Probe design

Probe measurements were carried out in the superheater region of the Rauma recovery boiler. The probe measurement location was located at the entrance to the tertiary superheater, close to the roof. Figure 23 shows a schematic of the convective section of the boiler indicating the sampling location.

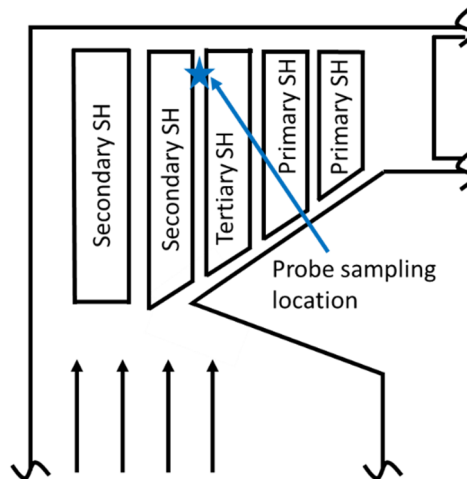


Figure 23: Schematic of convective section of Rauma kraft recovery boiler indicating sampling location

The probe consists of two concentric steel tubes. A detachable tip is used to collect the deposits. By this method, the deposits are still attached to the steel surface they formed on and can be collected and subsequently analyzed without separation from the steel. Thus, valuable information regarding the chemical composition and morphology of the deposit closest to the steel is obtained by this method. The steel temperature of the probe is constantly cooled to a designated temperature (representing the steel temperature of the nearby superheater tubes). Pressurized air is used to ensure cooling. The air enters the probe at the cold end, which is located outside of the boiler and exits the probe at the tip, directly into the flue gas stream in of the boiler. During the sampling period, steel temperature and flue gas temperature are measured and logged constantly (every five minutes). The logged steel temperature shown in Figure 24 indicates the temperature control system to be reliable under the conditions the probe is exposed to during the experiment. The average steel temperature for the five and eight-week experiment was 439.5 ± 6.2 °C and 460.5 ± 7.9 °C respectively.

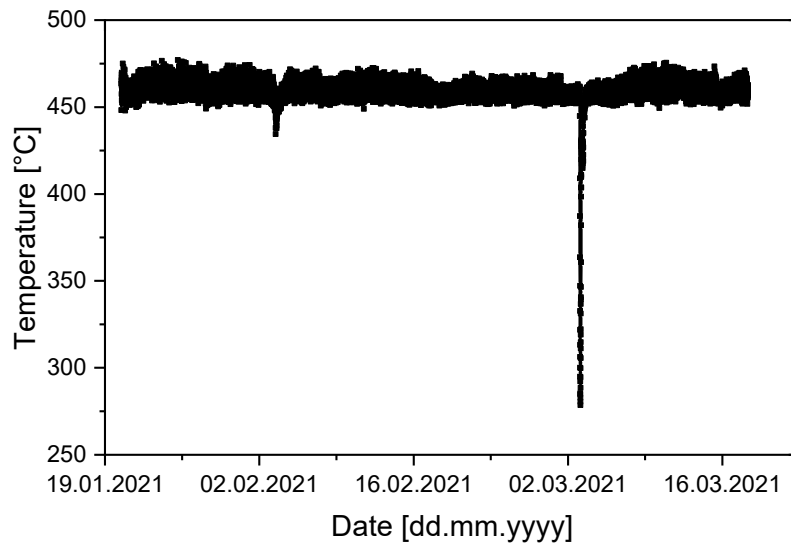


Figure 24: Logged probe steel temperature during eight week experiment

The boiler is accessed through an inspection hatch in the wall. A custom-designed plate is used to cover the opening during the measurements and to hold the probe in place. The high flue gas velocities and the regular sootblowing inside the boiler create a harsh environment within the boiler, which destroyed earlier probe designs. The current probe design has been developed based on several failure analyses and redesign cycles after unsuccessful measurement attempts. Figure 25 shows the general design of the probe, highlighting its main features.

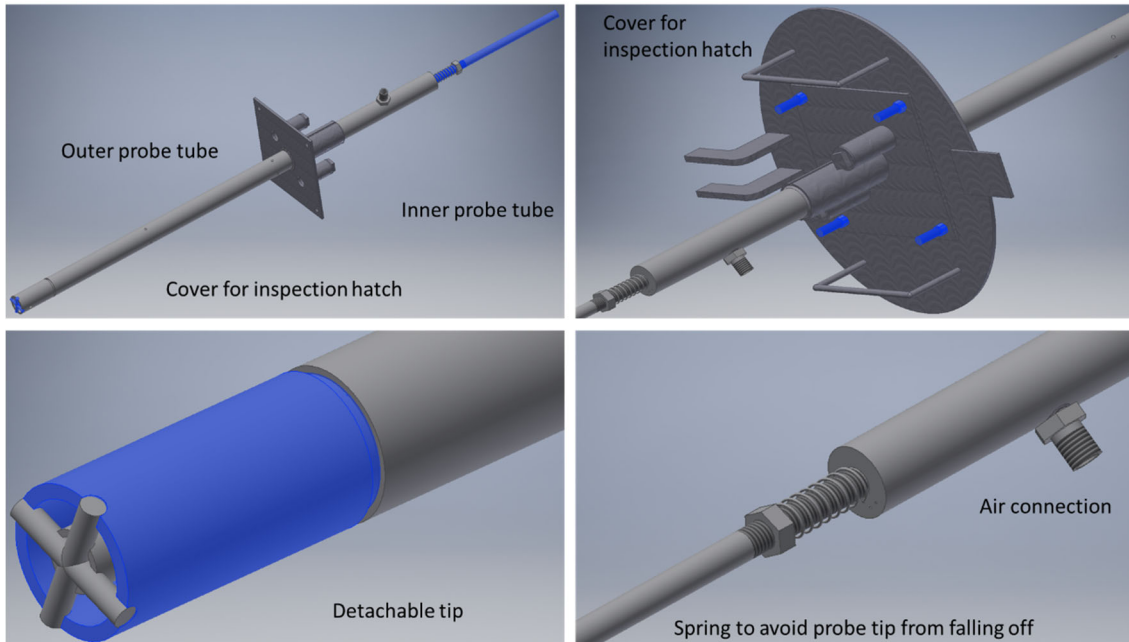


Figure 25: Key-features of probe design

A more detailed description of the probe design can be found in the appendix to this report. With the current probe design, aged deposits could be obtained after sampling periods of five and eight weeks. The probe has been damaged during the eight-week experiment, but this damage did not have any influence on the obtained deposit.

Sample analysis and key findings

Due to corrosion, the probe tip could not be removed easily from the main probe after the experiment has been ended. The best approach to remove the tip was to cut it off using a metal saw. Another approach to remove the tip by pulling it apart resulted in partial loss of material as some of the deposit fell off the probe. After the tip has been detached from the probe, the whole sample has been cast into epoxy resin to avoid any loss of material during transportation and also to avoid the deposit getting into contact with humid air causing any unwanted reactions that may alter the deposit properties. The samples are then cut to obtain a cross-section which is analysed using scanning electron microscopy and energy dispersive X-ray analysis. The location at which the probe samples were cut to obtain the cross-section was chosen to be at the location the thermocouple was located during sampling. Panorama images of the cross-sections of both deposits are shown in Figure 26

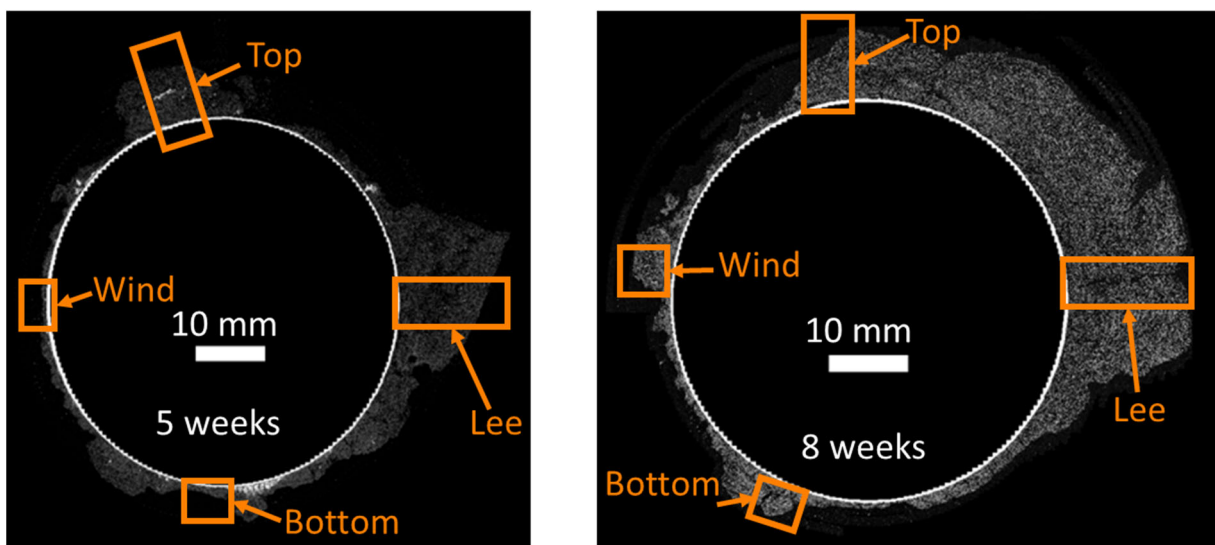


Figure 26: SEM images of cross-sections of probe deposit samples after exposure time of 5 weeks (left) and 8 weeks (right) including steel

The squares in Figure 26 indicate where elemental maps were taken from. The regions were chosen to get a good overview of the whole deposit samples and the different deposit morphologies and also ageing mechanisms that might be only observed specifically to a certain location. The deposition mechanisms for wind- and lee sides of superheater deposits are known to differ significantly. In addition, the bottom of the probe was directly facing the sootblower, which was located at a distance of 0.75 m below the probe. The part of the probe facing upward has been analyzed as well, as the deposit thickness has its maximum in this region.

Three, partially new, findings will be presented in more detail in this report. Besides, general observations made during the analysis of the samples will be presented more briefly as well. In addition to the two samples obtained within this project, analysis data from a third deposit sample obtained during an earlier measurement campaign with an exposure time of one week will be presented in this report as well.

General observations

Based on the data obtained from SEM/EDX analysis, the average Cl concentration within the samples of different exposure times could be calculated for the four analyzed locations along the cross-section of the probe. A summary of the average Cl content of the probe samples is presented in Figure 27

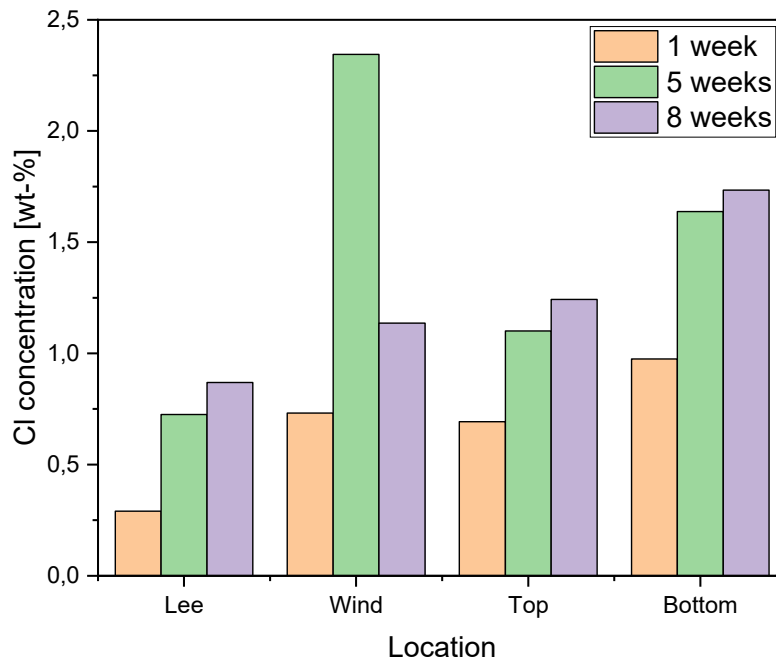


Figure 27: Average Cl concentration over time at analyzed locations of probe deposits of exposure times of 1, 5, and 8 weeks

From Figure 27 it becomes apparent that the average Cl content within the deposit increases over time. The enrichment does not seem to be location-specific as it can be seen at all four analyzed locations along the probe surface indicating that the overall deposit becomes enriched in Cl over time.

The deposit morphology appeared to be very similar to that of the previously obtained superheater deposits from the same boiler. No dense molten layer has been formed at any location within the deposits. This indicates that the deposits obtained from the probe measurements represent actual superheater deposits reasonably well. Nevertheless, the sampling location was very close to the boiler wall, which might have an impact on the local flue-gas flow properties.

In general, the morphology of the probe deposits is less structured compared to synthetic laboratory deposits. The synthetic laboratory deposits are very well structured, consisting of three distinct layers which can be separated by horizontal lines. The probe deposit sample, in contrast, has a more complex morphology. In Figure 28 SEM cross-sections of a synthetic laboratory deposit and a probe deposit are compared with each other.

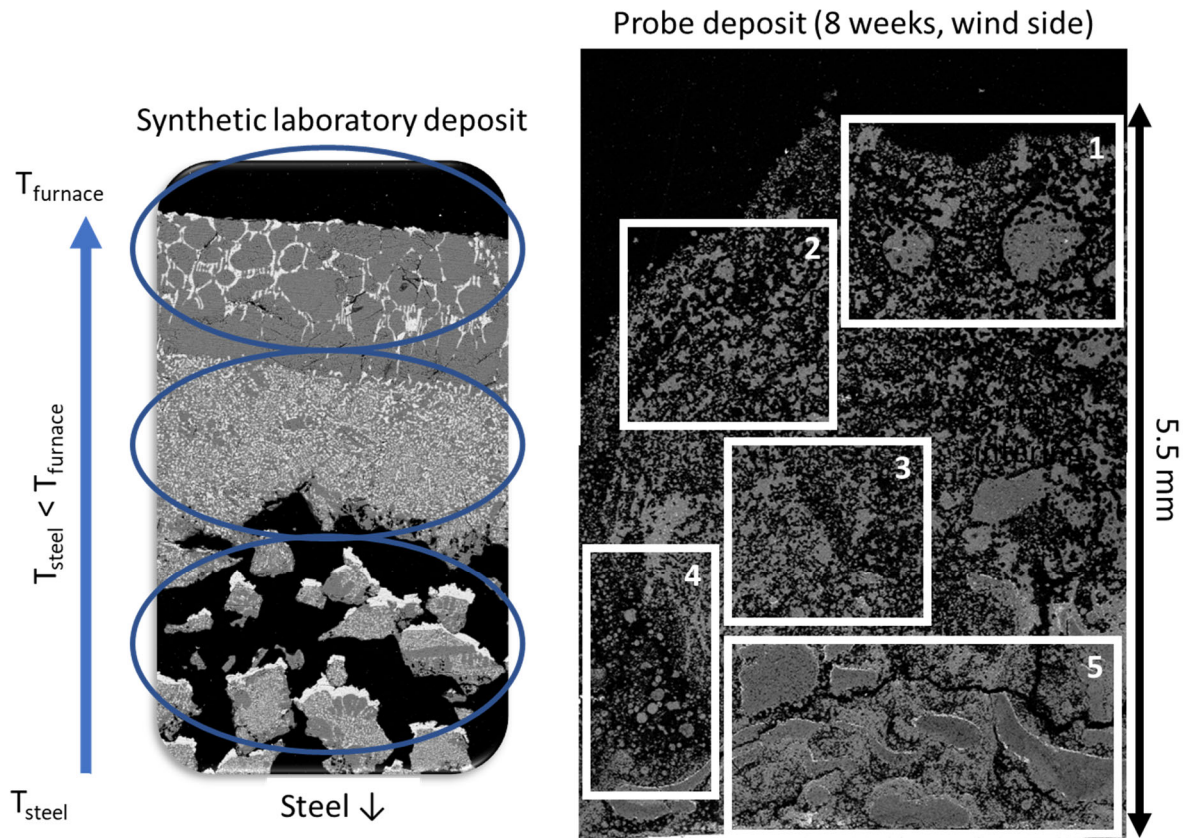


Figure 28: Morphological differences of synthetic laboratory deposit (left) and probe deposit sample (right)

As seen in Figure 28, several regions of different characteristics could be identified to be irregularly distributed throughout the cross-section of the probe deposit. The size of distinct particles within the probe deposit varies significantly among the highlighted regions. In region 1 of the probe deposit shown in Figure 28, several large particles can be identified while the particles in region 4 are significantly smaller. Furthermore, region 4 appears to be not sintered, while all the other highlighted regions in the image show varying degrees of sintering, which then also results in local changes of the deposit porosity. In addition, particles in region 5 appear to have been partially molten. Besides the observable differences shown in Figure 28 between the synthetic laboratory deposit and the probe sample, furnace conditions are significantly different for the two samples. In the laboratory, the furnace temperature is set to a fixed value and not affected by any further external influences, thus the temperature profile is very stable during the whole experimental time. In the boiler environment, on the other hand, the flue-gas temperature can vary as it is affected by various changes within the boiler environment. Sootblowing and changes in the boiler load can result in fluctuations in the flue-gas temperature. Furthermore, deposit shedding and erosion can result in changes in the local temperature gradient within the deposit over time. These possible fluctuations within the temperature gradient should be taken into account when analysing the probe deposits.

Formation of alkali chloride layers

In addition to the general enrichment of Cl within the samples, the formation of alkali chloride layers could be observed as well. Similar to the superheater deposits presented above in this report, the thickness of the formed alkali chloride layers was smaller compared to those observed in the laboratory experiments and also in the superheater deposits from the Brazilian kraft recovery boiler which has a higher Cl content in the deposits. Even after an exposure time of 8 weeks, the layer thickness did not increase significantly. But as the probe deposits are still attached to the steel surface

on which they initially formed, a statement can be made whether alkali chloride layer formation also takes place directly on the steel surface. In Figure 29 selected SEM images of the probe sample after an exposure time of 5 weeks are presented.

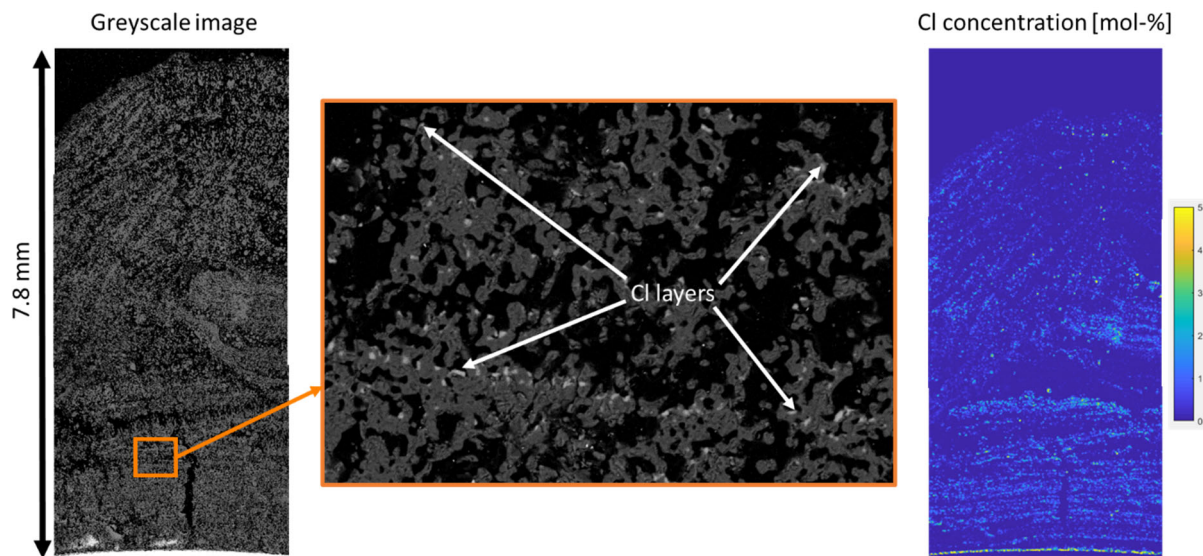


Figure 29: Alkali chloride layer formation on furnace facing side of particles (middle) and directly on steel surface (bottom of right image) after 5 week exposure time

As shown in Figure 29, alkali chloride layers were observed directly on the steel surface but also on the furnace-facing side of the particles within the deposit. Based on these observations it can be concluded that gaseous alkali chloride transport is responsible for the observed layer formation, meaning that this deposit ageing mechanism can increase the concentration of corrosive alkali chloride close to and directly on the steel surface.

Unlike the laboratory experiments and the superheater deposits collected from the superheater tubes, alkali chloride layers were not exclusively observed on the furnace facing side of particles within the probe deposit samples. In regions close to the steel, predominantly on the wind side of the deposits, particles were found to be fully surrounded by alkali chloride layers. Such layers, forming not exclusively on the furnace facing side of particles, were observed within all of the probe deposit samples (1, 5, and 8 weeks sampling period). Examples of such alkali chloride layers are shown in Figure 30.

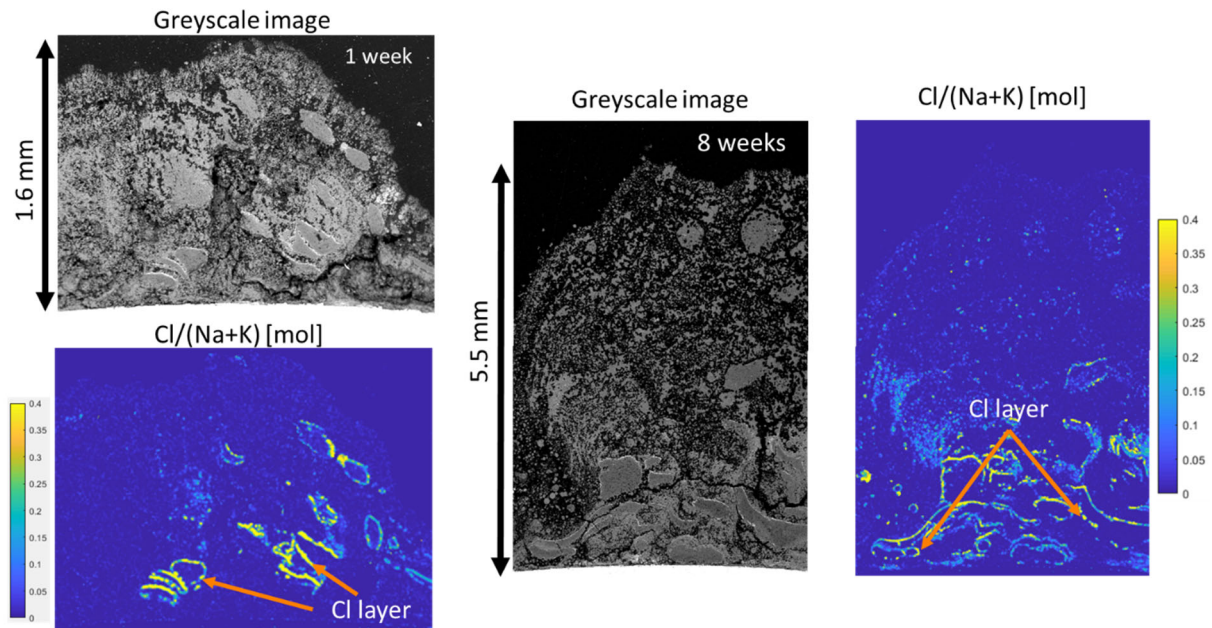


Figure 30: Cl-layers on non furnace facing side of particles of probe deposits after various exposure times

No definitive explanation for the observed formation of Cl layers on the non-furnace facing side of particles can be given at this point. Two factors that might result in the formation of these layers could be identified. Further research is needed to explain the Cl layer formation, observed in the probe deposits in detail. Similar observations could not be made in any of the previous laboratory experiments or the superheater deposits obtained directly from the superheater tubes. The two factors that might result in the observed formation of alkali chloride layers shown in Figure 30 will be explained in the following paragraphs.

A possible pathway for the observed alkali chloride layers to form is in-flight condensation of alkali chlorides on the surface of larger particles. In this case, the alkali chloride layer forms before deposition of the particle on the steel surface. This mechanism is an established deposit formation mechanism. As the first melting temperature of alkali chloride is lower than that of alkali sulfate and carbonate, a layer of condensed alkali chloride can form on larger solid particles in flight. This alkali chloride layer then increases the stickiness of the particles resulting in a higher probability of larger particles adhering to the steel surface if they are covered in an alkali chloride layer.

A second possible explanation for the formation of the observed alkali chloride layers could be connected to the melting behaviour of the deposit particles. Due to the low Cl content of the deposits, the amount of melt formed at the first melting temperature is relatively low and does not increase significantly with increasing temperature. Thus, the amount of melt present is not sufficient for it to start filling the pores and moving toward the steel due to capillary forces. The small amounts of melt formed under operational conditions are expected to rather accumulate around the original particles as partial melting takes place. Due to the high surface tension of the melt, a layer surrounding the whole original particle develops.

Dense melt-like structures close to steel surface

The second major observation made when analyzing the probe deposit samples was the occurrence of dense melt-like structures that could be found in direct vicinity of the steel surface, mainly on the wind

and bottom side of the probe deposit. Examples of such particles close to the steel surface are presented in Figure 31

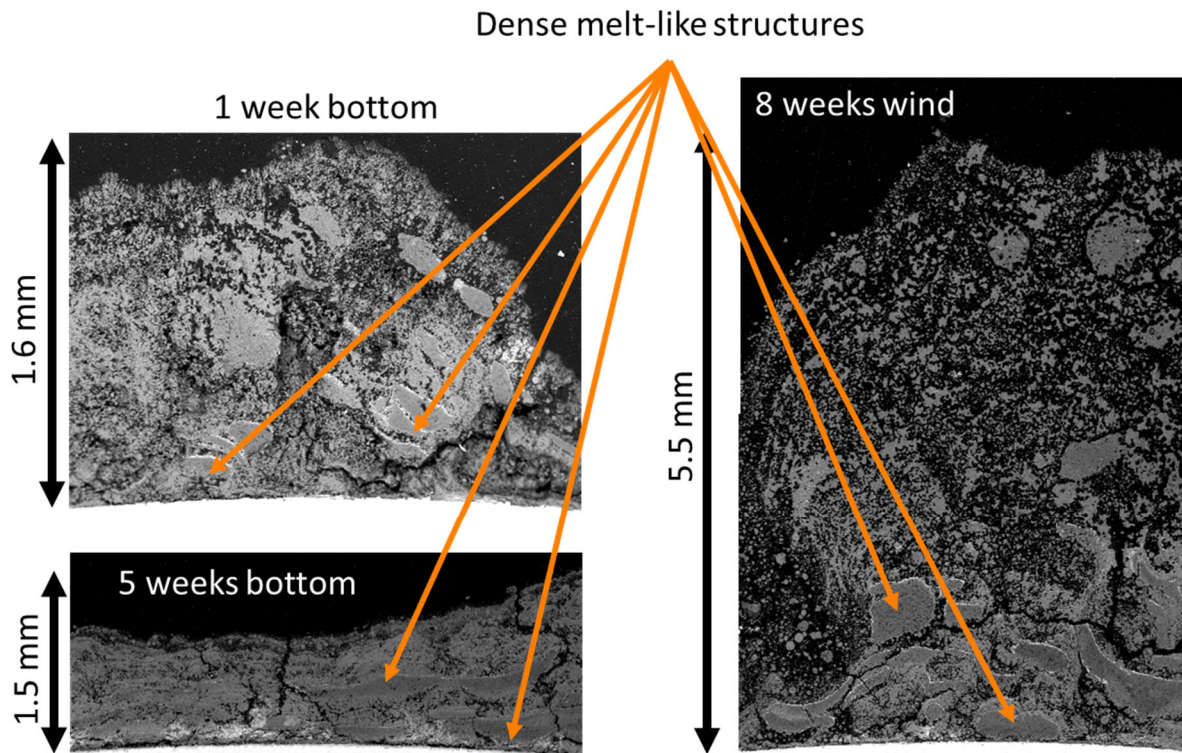


Figure 31: SEM images showing dense melt-like structures close to steel surface of probe deposits

The fact that these particles were mainly observed on the wind side and the bottom of the probe, might be an indication for carry-over particle deposition. The influence of the sootblower, especially on the bottom of the probe, on the formation of the observed particles is not known at this point. The temporarily increased water vapour concentration in the flue-gas might result in partial dissolution of the water-soluble deposit, which crystallizes subsequently forming the large agglomerates shown in Figure 31

The composition of the dense, melt-like structures was further analyzed utilizing SEM/EDX data. The results of the analysis are shown in Figure 32

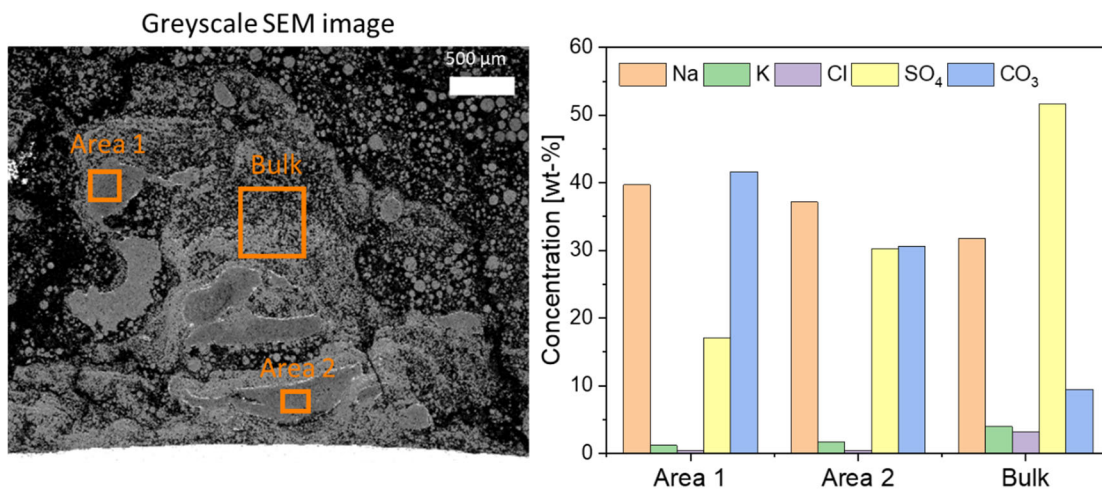


Figure 32: Area analysis of dense melt-like structures in probe deposits

As seen in Figure 32, the dense structures are depleted in K compared to the surrounding deposit material. At the same time, the carbon content of the dense structure is higher compared to the bulk deposit. The carbon content is not measured directly in the SEM analysis but is calculated by closing the charge balance in Equation (1).

$$n(\text{Na})+n(\text{K})=n(\text{Cl})+2n(\text{S})+2n(\text{C}) \quad (1)$$

The SEM data strengthens the interpretation of the dense melt-like structures being carry-over material.

Dense, melt-like deposit structures could also be observed in the superheater deposits from the Rauma kraft recovery boiler. Only deposits collected at the inlet of the tertiary superheater tubes contained similar dense melt-like formations, while within deposits collected at the exit of the tertiary superheater these structures could not be seen. The observations from the superheater deposits further increase the possibility of the dense melt-like structures being carry-over material.

K and S enrichment closest to the steel

A third phenomenon, that has already been observed previously in the superheater deposits (“type 2” Finnish boiler deposit) can also be seen in the probe deposits. Closest to the steel, regions enriched in K and SO₄ can be seen. This K and SO₄ enriched region of the deposit is at the same time depleted in Cl. It is expected that the observations made within the probe measurements are based on the same formation mechanism as in the superheater deposits, which is not known to this point. The probe measurements gave some additional information regarding the simultaneous K and S enrichment, as it could only be observed within the upward-facing part of the probe deposit. Furthermore, the K and S enrichment could already be seen after an exposure time of only one week, indicating that the formation mechanism of this phenomenon likely takes place during the early stages of deposit build-up. But compared to the superheater deposits presented above (Figure 20), the K and S enrichment is

less pronounced in the probe deposit samples. A comparison of a probe and superheater deposit sample is shown in Figure 33.

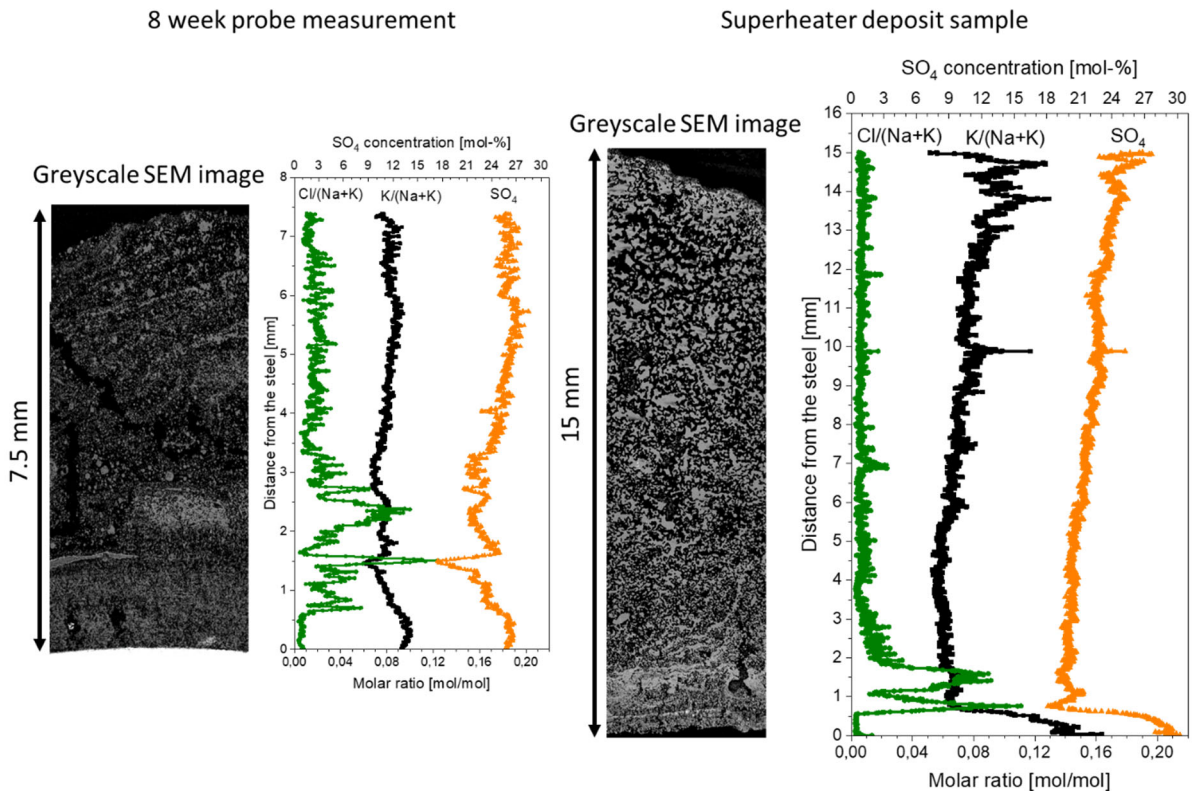


Figure 33: K, Cl, and SO₄ concentration through cross-section of probe deposit (left) and superheater deposit (right), both deposit samples taken from the Rauma boiler

One possible explanation of the observed differences, at least to some extent, is the significantly lower SO₂ concentration measured in the flue-gas stack during the probe sampling period compared to the measured concentration during the superheater deposits built-up. The differences in the SO₂ concentration are connected to the fact that the probe measurements are carried out during regular boiler operation. Being able to start and end experiments during regular boiler operation is a major advantage of the probe sampling method as no boiler shut-down is needed to insert or remove the probe from the boiler environment. But on the other hand, the initial deposit formation mechanisms on the probe surface might differ from those on actual superheater tubes, as the used fuel and the superheater steel temperatures during the start-up period of the boiler might differ from conditions during regular operation.

The K and S enriched regions occurring only on the upward-facing side of the deposits might be an indication that certain deposition mechanisms or flow conditions, that only occur on the upward-facing side of the probe, are required to form the observed K and S enriched region within the deposit.

It is currently not known whether and if so to what extent this phenomenon within deposits will affect boiler operation and corrosion. Further research is needed to investigate the role of Cl connected to the observed K and S enrichment. One possible approach to further study this phenomenon would be to carry out probe measurements during the boiler start-up and compare the results with probe deposits of the same exposure time that have been obtained during regular boiler operation.

Analogous to the superheater deposit, the impact of the local K enrichment on the first melting temperature was analyzed for the probe deposit as well. In Figure 34 the local T₀ profile for the probe deposit is shown together with a SEM image indicating the sections the deposit was divided into.

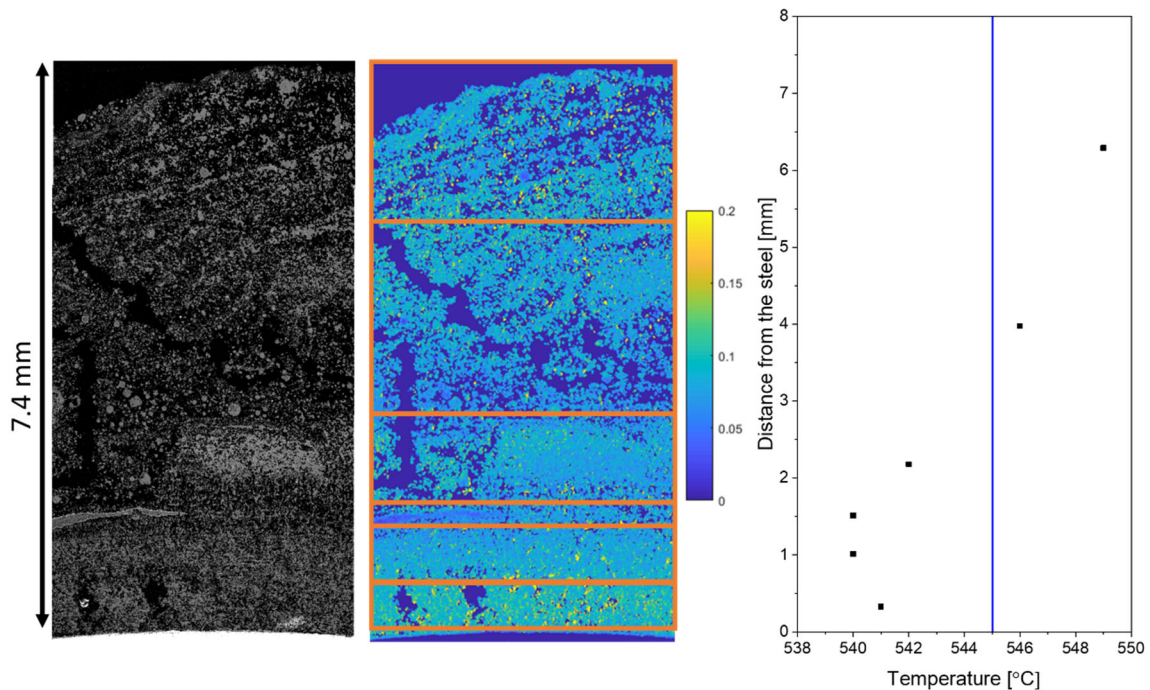


Figure 34: Local first melting temperature of "Type 2" like probe deposit of 8 weeks exposure time

As shown in Figure 34, the region enriched in K shows a minimum in the local first melting temperature. The results are in agreement with the above-presented superheater deposits of "Type 2".

Local first melting temperature within probe deposits

Besides the region of the probe deposit resembling a "Type 2" superheater deposit, profiles of the local first melting temperature have been calculated for the other analyzed locations along the deposit cross-section as well. The profiles presented in the following chapter show the results of the probe deposit with an exposure time of 8 weeks. No T_0 profile has been calculated for the bottom side of the probe deposit, as the thickness of the deposit was not sufficient to reasonably divide the deposit into several sections.

Starting with the deposit on the wind side of the probe, which has larger molten agglomerates close to the steel surface that are surrounded by a Cl rich layer. The SEM images showing the molar Cl/(Na+K) and K/(Na+K) distribution within these samples and the graphs showing the average molar ratios as function of distance from the steel are shown in Figure 35 together with the local T_0 profile of the deposit.

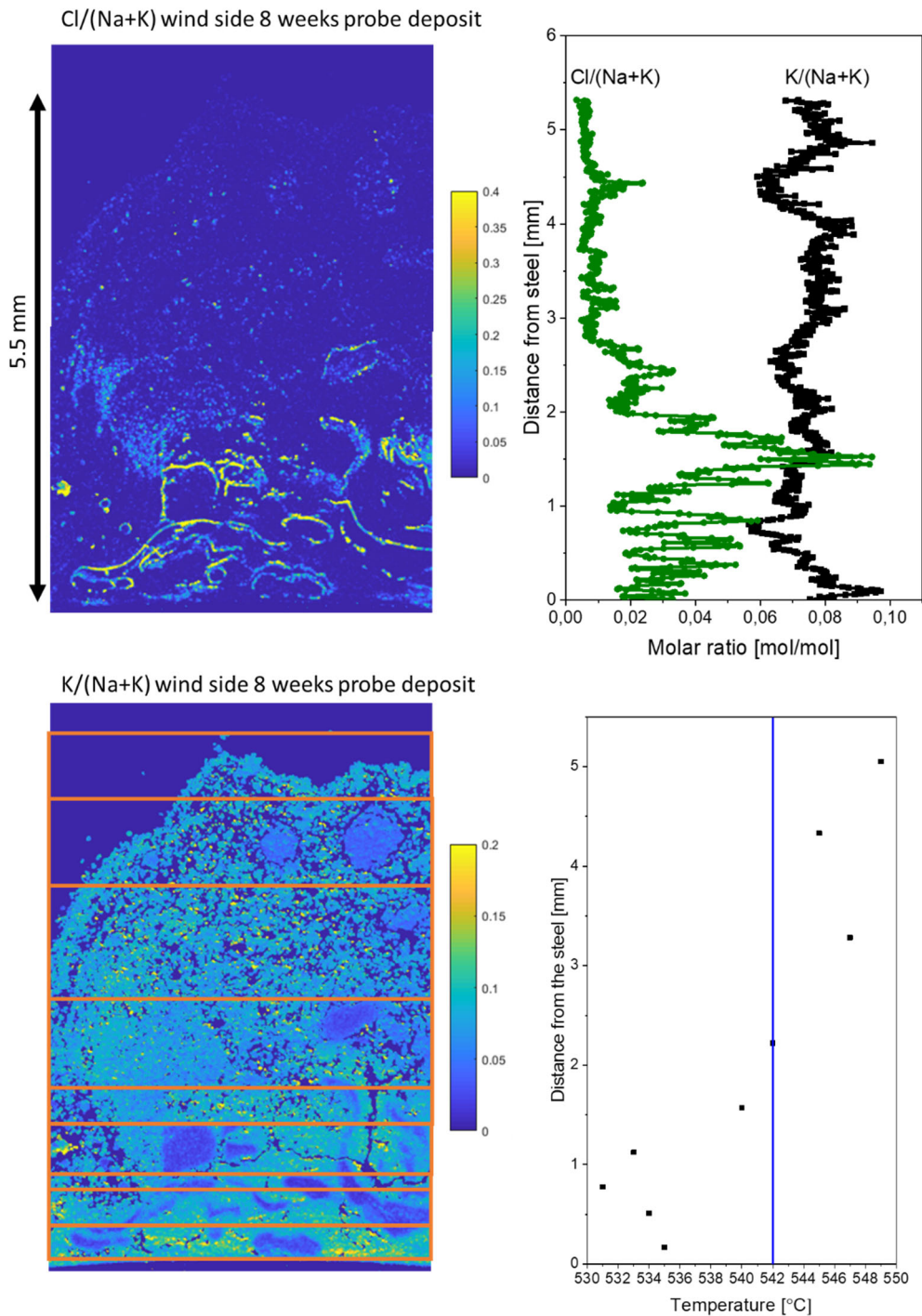


Figure 35: SEM images depicting molar Cl/(Na+K) and K/(Na+K) ratios, graphs of average molar ratios as function of distance from the steel and local T_0 profile

From the graphs in Figure 35 showing the average molar ratios as function of distance from the steel, it can be seen that the region of the deposit consisting of larger agglomerates, close to the steel, is enriched in Cl compared to the bulk deposit. But only a small layer closest to the steel is also enriched in K when compared to the bulk deposit. Nevertheless, the local T_0 values within the whole layer of dense molten particles are lower compared to the bulk deposit T_0 .

The next section of the probe deposit to look at is the lee side of the probe. The maximum deposit thickness after the sampling period of eight weeks has been recorded at the lee side of the deposit, with 15.6 mm. The majority of the deposit consists of a layer of larger, sintered agglomerates with a rather constant Cl and K concentration. Toward the steel, the deposit contains a higher amount of distinct spherical particles. In the region closest to the steel, the deposit is slightly enriched in Cl compared to the outer region. The K content throughout the whole deposit cross-section is fairly constant. A SEM image of the grey-scale cross-section of the lee side deposit together with images depicting the Cl/(Na+K) and K/(Na+K) ratios are shown in Figure 36.

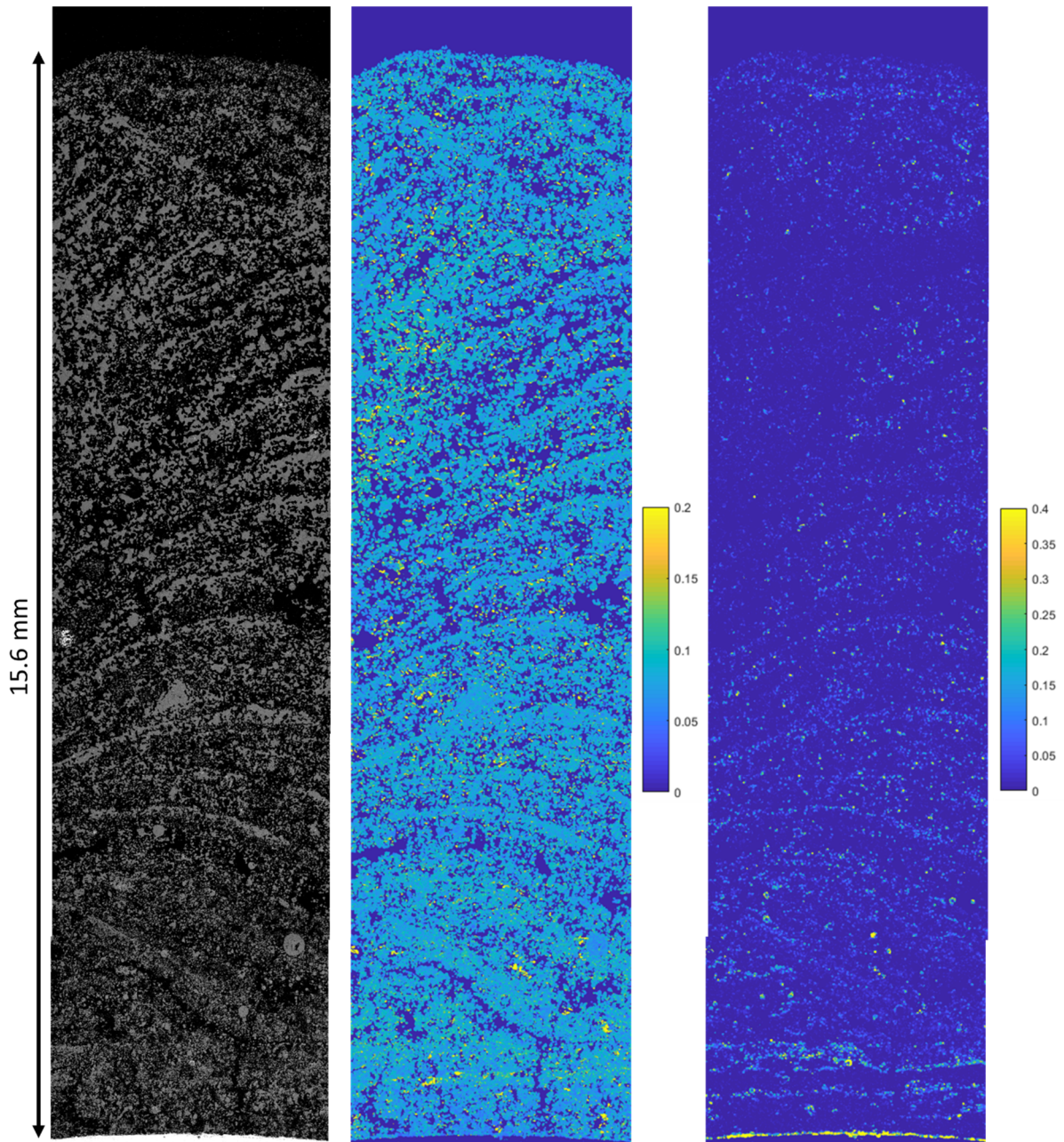


Figure 36: Greyscale SEM image of lee side of 8 week probe deposit (left), molar $K/(Na+K)$ middle, and molar $Cl/(Na+K)$ right

The enrichment in Cl and K within the lee side of the deposit is relatively small, thus the sections the deposit has been divided into to calculate the local first melting temperature have been chosen to be larger for this deposit compared to the other cross-sections. The SEM image of the molar $Cl/(Na+K)$ indicating the sections of the deposit has been divided into is presented in Figure 37 together with the average $Cl/(Na+K)$ and $K/(Na+K)$ ratios and the local T_0 profile of the deposit.

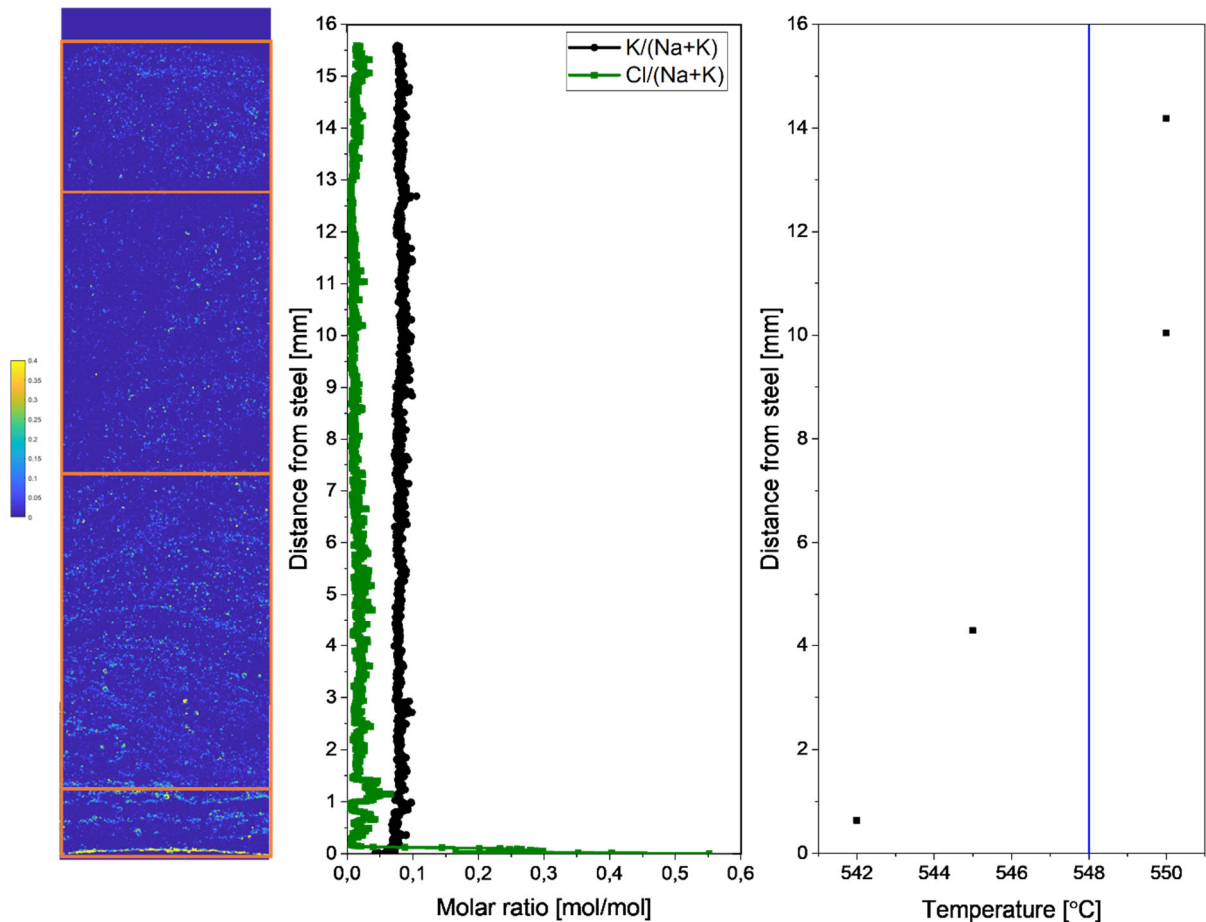


Figure 37: SEM image of molar Cl/(Na+K) ratio indicating the sections the deposit has been divided into (left), average Cl/(Na+K) and K/(Na+K) ratios as function of distance from the steel (middle), and local T_0 profile (right) of lee side probe deposit after eight weeks exposure time

Similar to the deposit on the wind side, the local first melting temperature is locally decreased compared to the bulk deposit in the sections close to the steel. Even though no significant enrichment in K could be observed within this region of the deposit. When comparing wind and lee sides, the wind side probe deposit sample (Figure 35) has lower local T_0 values as compared to the T_0 values in the lee side deposit.

The analysis of the local melting behaviour of the probe deposit is in line with the analysis carried out earlier concerning the laboratory and full-scale superheater deposits. Toward the steel, the first melting temperature is lower compared to the T_0 of the bulk deposit. Even within regions of the deposit that did not show any significant K enrichment. It is worthwhile mentioning here, that the local decrease in T_0 was more pronounced if the deposit was enriched in K, especially if the enrichment was caused by movement of melt. It can be concluded that deposit ageing mechanisms are likely to locally decrease the first melting temperature of deposits and the extent to which T_0 is decreased is dependent on the predominating ageing mechanism.

Conclusions

Based on all results presented in the report above, it can be concluded that the probe measurements proved to be a reasonable experimental approach to study superheater deposits and especially deposit ageing. The probe measurements provide important data as the exposure time can be varied and determined independently of the recovery boiler operation.

The probe measurements carried out in the present measurement campaign, but also previous shorter probe measurements (phase 1) complement the data from earlier laboratory experiments and full-scale superheater deposit sampling very well. The results of the probe measurements are well in line with the earlier experimental results, showing the same deposit ageing mechanisms, which have been identified in previous laboratory experiments.

Based on the overall body of knowledge gained from laboratory experiments, boiler deposit sampling, and probe measurements it can be concluded that Cl enrichment in Finnish superheater deposits takes place with time. Both local enrichment, forming Cl-rich layers within the deposit, but also a general increase in the bulk Cl content of the deposits takes place over time.

Both boiler deposit samples and probe deposits show a local decrease in T_0 close to the steel compared to the bulk deposit. The composition differences resulting in these locally lower T_0 values can either be set up during initial deposit build-up stages (condensation of alkali chloride vapours on steel surface) and/or due to time-dependent changes within the deposit after the deposit has built up. In both cases, the mechanism is vaporization-condensation of alkali chlorides and can be expected to increase the risk of corrosion with time.

In Finnish mill deposits, vaporization and condensation and gas-phase alkali chloride transport appear to be the main mechanism by which the deposit can be enriched in alkali chlorides, both locally and as a whole. In contrast, Brazilian deposits have higher Cl compared to typical Finnish/Scandinavian mills. The higher Cl of Brazilian deposits results in additional deposit ageing mechanisms becoming relevant. In the Brazilian deposits studied, movement of an alkali chloride-rich melt toward the steel resulted in locally lower T_0 values toward the steel. In addition, gas phase alkali chloride transport could clearly be seen to have taken place in the Brazilian deposits as well. The lowest local T_0 value found in the Brazilian deposits (517 °C) was slightly lower as compared to the lowest T_0 value in the Finnish superheater deposit (522 °C). In both the Brazilian and Finnish superheater deposits, the lowest local T_0 values were typically found in the region relatively close to the steel surface.

The Rauma probe measurements also provided observations of new deposit characteristics to be understood better in future work. Similar observations were also made in the deposit samples collected directly from the superheaters in the Rauma boiler.

Parts of the probe deposits and some of the boiler superheater deposits show formation of a K and SO_4 enriched region which is expected to be connected to sulfation of alkali chloride, and the formation of dense melt-like structures close to the steel. Better understanding of these observations requires further investigation. Measurements could be carried out during boiler start-up in the future to investigate the sulfation reaction in more detail and start-up effects on deposit ageing in general.

- [1] Tran HN, Reeve DW, Barham D. Formation of kraft recovery boiler superheater fireside deposits. *Pulp & Paper Canada* 1983;84:T7–12.
- [2] Frederick WJ, Vakkilainen EK. Sintering and Structure Development in Alkali Metal Salt Deposits Formed in Kraft Recovery Boilers. *Energy and Fuels* 2003;17:1501–9. <https://doi.org/10.1021/ef034012s>.
- [3] Baxter L, Hatch G, Sinquefield SA, Frederick WJ. An experimental study of the mechanisms of fine particle deposition in kraft recovery boilers. 2004 International Chemical Recovery Conference 2004;1:393–412.
- [4] Mikkanen P. Fly ash particle formation in kraft recovery boilers. 2000.
- [5] Vakkilainen EK. Kraft recovery boilers - Principles and practice. Suomen Soodakattilayhdistys r.y.; 2005.
- [6] Isaak P, Tran HN, Barham D, Reeve DW. Stickiness of Fireside Deposits in Kraft Recovery Units. *Journal of Pulp and Paper Science* 1986;12:84–8.
- [7] Mao X, Kuhn DCS, Backman R, Hupa M. The sticky temperature of recovery boiler fireside deposits. *Pulp & Paper Canada* 2002;103:29–33.
- [8] Reeve DW, Tran HN, Barham D. The effluent-free bleached kraft pulp mill - Part XI Morphology, chemical and thermal properties of recovery boiler superheater fireside deposits. *Pulp & Paper Canada* 1981;82.
- [9] Frederick WJ, Vakkilainen EK. Sintering and Structure Development in Alkali Metal Salt Deposits Formed in Kraft Recovery Boilers. *Energy and Fuels* 2003;17:1501–9. <https://doi.org/10.1021/ef034012s>.
- [10] Tran H. Recovery boiler fireside deposits and plugging prevention. TAPPI Kraft Recovery Course 2007 2007;2:537–72.
- [11] Broström M, Enestam S, Backman R, Mäkelä K. Condensation in the KCl-NaCl system. *Fuel Processing Technology* 2013;105:142–8. <https://doi.org/10.1016/j.fuproc.2011.08.006>.
- [12] Lindberg D, Engblom M, Yrjas P, Laurén T, Lindholm J, Hupa M. Influence of deposit aging on superheater corrosion. 2014 International Chemical Recovery Conference, 2014, p. 101–13.
- [13] Reeve DW, Tran HN, Barham D. Superheater Fireside Deposits and Corrosion in Kraft Recovery Boilers. *Tappi* 1981;64:109–13.
- [14] Costa A, Silva D, Abelha F, Cenibra CNSA. EXPERIENCE OF RECOVERY BOILER SUPERHEATER CORROSION AT CENIBRA. International Chemical Recovery Conference, 2017.
- [15] Balint R, Engblom M, Niemi J, Silva da Costa D, Lindberg D, Yrjas P, et al. Temperature gradient induced changes within superheater ash deposits high in chlorine. *Energy* 2021;226:120439. <https://doi.org/10.1016/j.energy.2021.120439>.
- [16] Reeve DW, Tran HN, Barham D. Superheater Fireside Deposits and Corrosion in Kraft Recovery Boilers. *Tappi* 1981;64:109–13.
- [17] Niemi J, Lindberg D, Engblom M, Hupa M. Simultaneous melt and vapor induced ash deposit aging mechanisms – Mathematical model and experimental observations. *Chemical Engineering Science* 2017;173:196–207. <https://doi.org/10.1016/j.ces.2017.07.041>.

- [18] Niemi J, Balint R, Engblom M, Lehmusto J, Lindberg D. Temperature-Gradient-Driven Aging Mechanisms in Alkali-Bromide- And Sulfate-Containing Ash Deposits. *Energy and Fuels* 2019;33:5883–92. <https://doi.org/10.1021/acs.energyfuels.8b04199>.
- [19] Lindberg D, Niemi J, Engblom M, Yrjas P, Laurén T, Hupa M. Effect of temperature gradient on composition and morphology of synthetic chlorine-containing biomass boiler deposits. *Fuel Processing Technology* 2016;141:285–98. <https://doi.org/10.1016/j.fuproc.2015.10.011>.
- [20] Niemi J, Engblom M, Laurén T, Yrjas P, Lehmusto J, Hupa M, et al. Superheater deposits and corrosion in temperature gradient – Laboratory studies into effects of flue gas composition, initial deposit structure, and exposure time. *Energy* 2021;228. <https://doi.org/10.1016/j.energy.2021.120494>.
- [21] Pfann WG. Zone Melting - This technique offers unique advantages in purification and in control of composition in various substances. *Science* 1962;135:1101–9. <https://doi.org/10.1126/science.135.3509.1101>.
- [22] Rettenmayr M. Melting and remelting phenomena. *International Materials Reviews* 2009;54:1–17. <https://doi.org/10.1179/174328009X392930>.
- [23] Lozovskii VN, Popov VP. Temperature gradient zone melting. *Progress In Crystal Growth And Characterization* 1983;6:1–23. [https://doi.org/10.1016/0146-3535\(83\)90022-9](https://doi.org/10.1016/0146-3535(83)90022-9).
- [24] Lograsso TA, Hellawell A. Temperature gradient zone melting: Approach to steady state. *Journal of Crystal Growth* 1984;66:531–40. [https://doi.org/10.1016/0022-0248\(84\)90151-9](https://doi.org/10.1016/0022-0248(84)90151-9).
- [25] Bale CW, Bélisle E, Chartrand P, Deckerov SA, Eriksson G, Gheribi AE, et al. FactSage thermochemical software and databases, 2010-2016. *Calphad: Computer Coupling of Phase Diagrams and Thermochemistry* 2016;54:35–53. <https://doi.org/10.1016/j.calphad.2016.05.002>.
- [26] Mao X, Lee S, Tran H. Effects of Carryover Liquid Content and Particle Size on Deposit Removability in Kraft Recovery Boilers. *Journal of Pulp and Paper Science* 2009;35:41–5.
- [27] Cardoso M, de Oliveira ÉD, Passos ML. Chemical composition and physical properties of black liquors and their effects on liquor recovery operation in Brazilian pulp mills. *Fuel* 2009;88:756–63. <https://doi.org/10.1016/j.fuel.2008.10.016>.
- [28] Zbogor A, Frandsen FJ, Jensen PA, Glarborg P. Heat transfer in ash deposits: A modelling tool-box. *Progress in Energy and Combustion Science* 2005;31:371–421. <https://doi.org/10.1016/j.pecs.2005.08.002>.
- [29] Boonsongsup L, Iisa K, Lu Y. Sulfation of Potassium Chloride at Combustion Conditions. *Industrial & Engineering Chemistry Research* 1997;36:4212–6. <https://doi.org/10.1021/ef990057a>.

Detailed description of probe design

The final probe design consists of an outer tube with a diameter of 51 mm. The length of the probe inside the boiler during sampling is 854 mm, including the detachable tip which has a length of 100 mm. The main purpose of the inner tube is to prevent the tip from detaching and falling off the main probe during the experiment. Therefore, 4 notches are implemented in the tip where the inner tube can fit in, pulling the tip toward the main probe and hindering the tip not only from detaching from the main probe but also from rotating during sampling. Figure 38 depicts the tip attached to the main probe with the inner metal tube holding it in place.

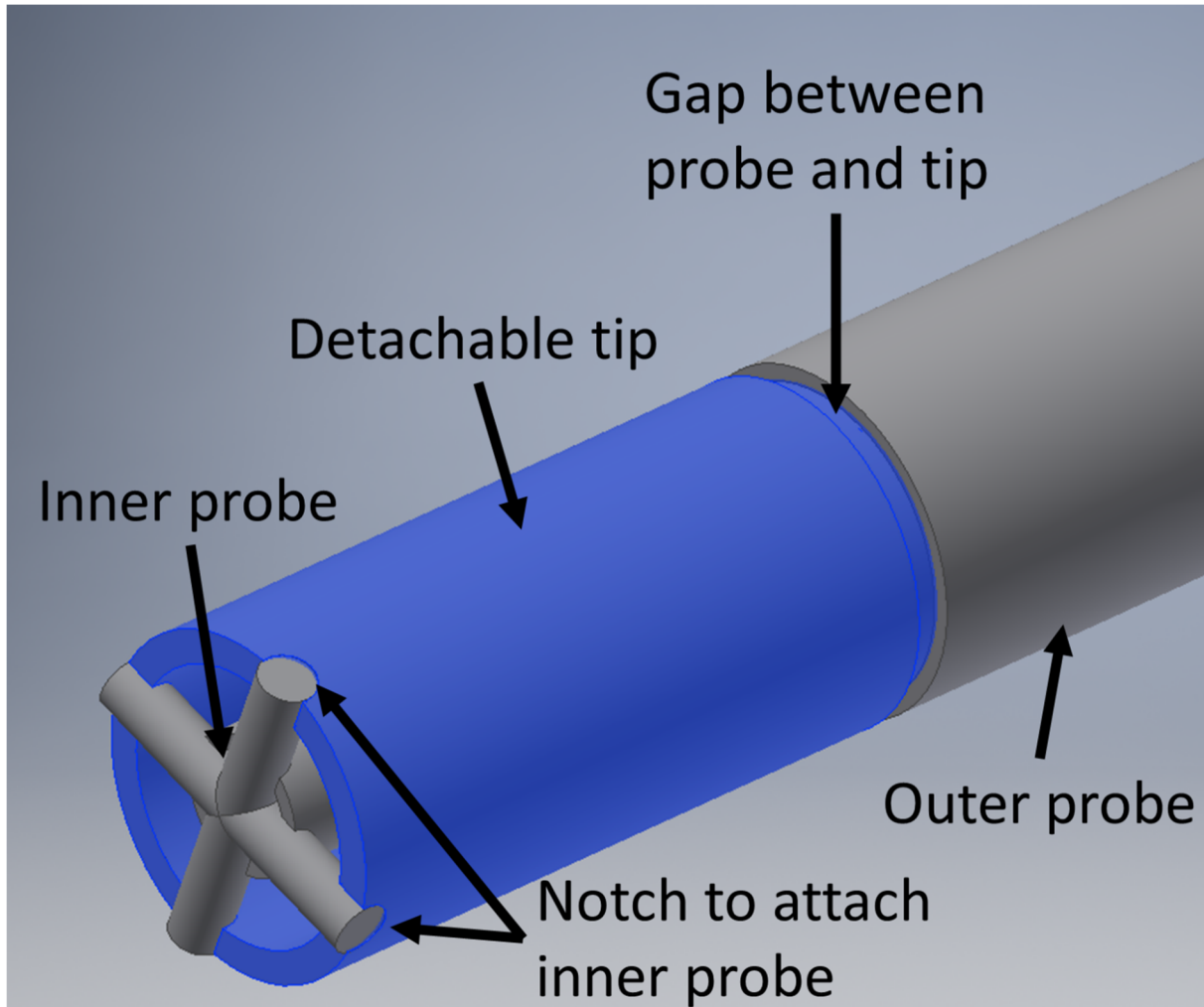


Figure 38: Detachable probe tip

A small gap is placed between the outer probe and the detachable tip. Previous experiments showed that removing the tip after the sampling period can be difficult due to corrosion. Thus a lot of force was required to remove the tip which resulted in heavy shaking and partial destruction of the deposit while removing the tip. The small gap aims to facilitate removal of the tip. If the tip cannot be removed at all due to corrosion, it is possible to use a metal saw to cut off the tip at the gap without destroying the main probe.

Cooling of the probe is ensured by pressurized air. Within the detachable tip, 2 thermocouples are located. One to control the steel temperature and the second one to log the temperature constantly. The airflow of the cooling air is adjusted by a control box which is connected to one of the

thermocouples inside the probe tip. Cooling air enters the probe at the cold end, passes through the probe between the inner and outer probe, and is subsequently blown into the boiler after exiting the probe at the tip. This ensures a constant steel temperature throughout the whole sampling period. The back end of the probe, which is located outside of the boiler during the sampling is shown in Figure 39.

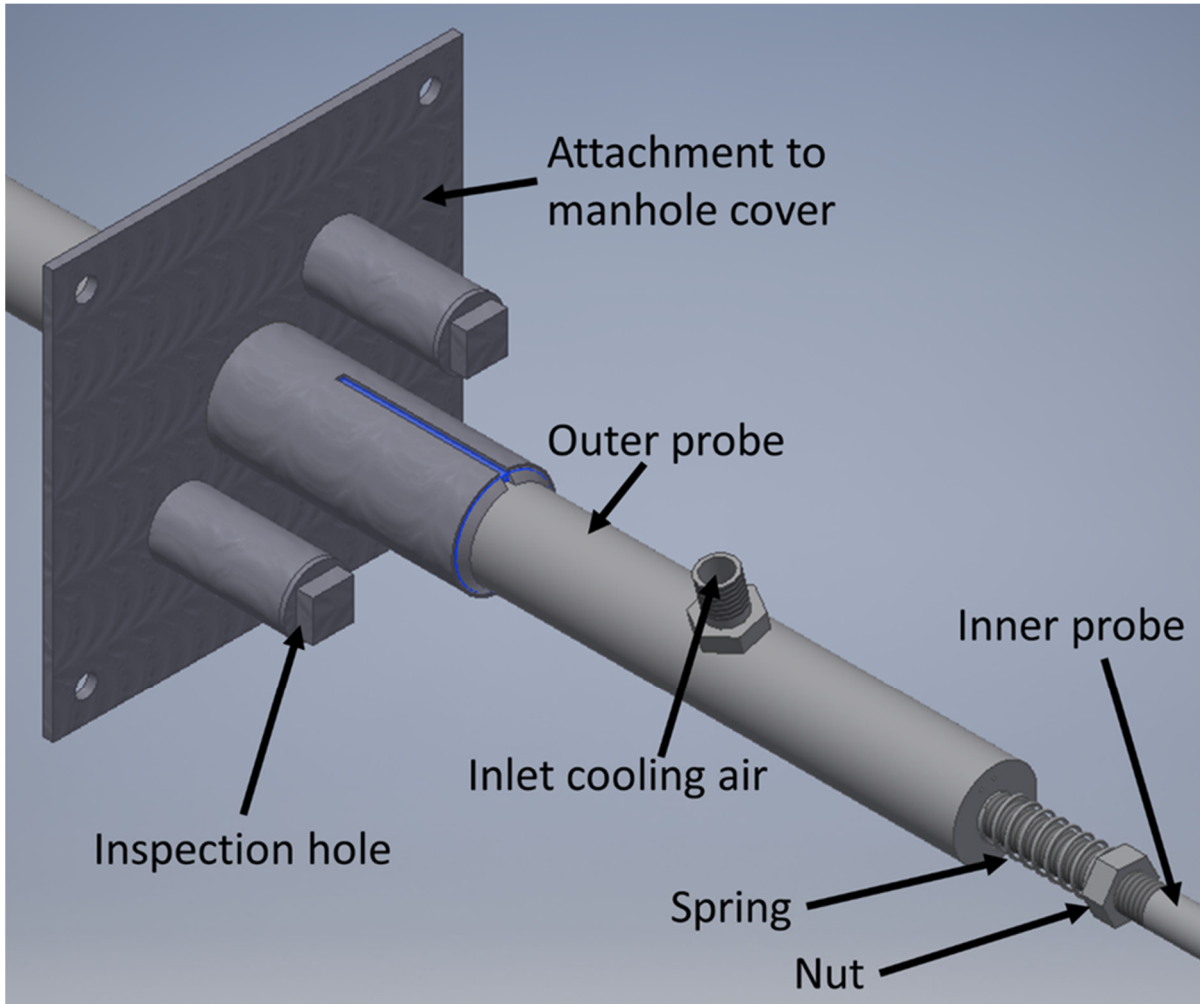


Figure 39: Back end of the probe located outside of the boiler during sampling period

The whole probe is welded to the rectangular plate shown in Figure 39, which is then attached to the manhole cover during the sampling period. Two inspection holes are located on the rectangular plate. During the sampling period, a thermocouple is inserted into the boiler through one of the inspection holes to log the flue gas temperature. By welding the probe to the rectangular plate, rotation during the sampling period should be avoided. At the back end of the probe, a spring is used to build up enough force for the inner probe to attach the tip to the main probe. By using a spring, irregular degrees of thermal extension of the inner and outer probe can be compensated. As the outer probe is directly exposed to the hot flue-gases, the steel temperature can be expected to be higher than the inner probe, thus the thermal extension of the inner probe is assumed to be smaller than that of the outer probe.

After the sampling period, the probe is removed from the boiler together with the rectangular plate. The opening in the manhole cover is square shaped with an edge length of 150 mm. It can be assumed that the size of this opening is sufficiently big to remove the probe from the boiler without destroying the deposit.

The manhole cover is shown in Figure 40.

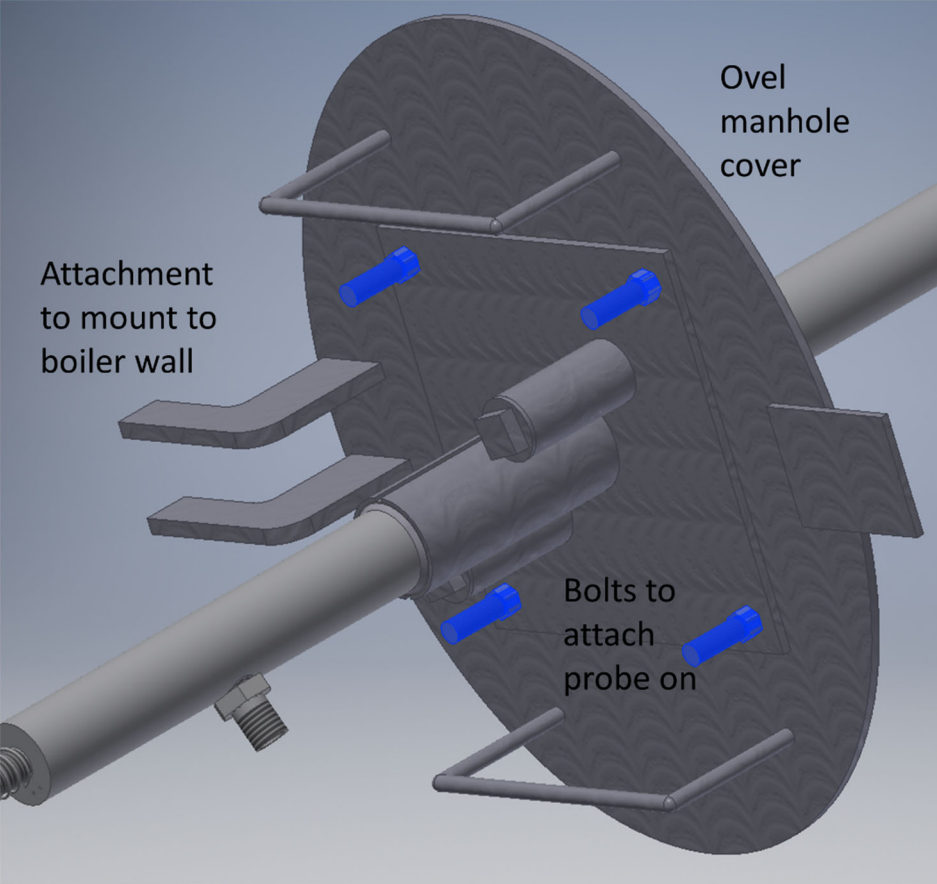


Figure 40: Oval manhole cover plate with probe attached to it

The oval plate has been designed to exactly fit the opening in the specific boiler the measurements were carried out in. The plate is attached to the boiler wall utilizing the mechanism that is used to close the manhole usually and the other side is jammed between the boiler wall and hinge of the inspection hatch opening.